AD-A047 261   MICHIGAN UNIV ANN ARBOR DEPT OF NAVAL ARCHITECTURE --ETC F/G 20/4
                OPTIMAL STOCHASTIC PATH CONTROL OF SURFACE SHIPS IN SHALLOW WAT--ETC(U)
                AUG 77   M G PARSONS, H T CUONG   N00014-76-C-0751
UNCLASSIFIED   189   ONR-CR215-249-2F   NL

END
DATE
FILMED
1-78
DDC

AD A047261

REPORT ONR-CR215-249-2F

18 19

12
B.S.

OFFICE OF
USN ONR
NAVAL RESEARCH

6

OPTIMAL STOCHASTIC PATH CONTROL
OF SURFACE SHIPS IN SHALLOW WATER

D D C
RECEIVED
DEC 5 1977
F

10   MICHAEL G. PARSONS
HUA TU CUONG

DEPARTMENT OF NAVAL ARCHITECTURE AND MARINE ENGINEERING
THE UNIVERSITY OF MICHIGAN
ANN ARBOR, MICHIGAN   48109

15   CONTRACT N00014-76-C-0751   12 88 p.

11   15 AUGUST 1977

7   FINAL REPORT.   1 MAY 76 — 30 JUNE 77

14 189

Approved for public release; distribution unlimited.

AD No. ____
DDC FILE COPY

PREPARED FOR THE

OFFICE OF NAVAL RESEARCH·800 N. QUINCY ST.·ARLINGTON·VA·22217

401 188

NOTICES

Change of Address

Organizations receiving reports on the initial distribution list should confirm correct address. This list is located at the end of the report. Any change of address or distribution should be conveyed to the Office of Naval Research, Code 211, Arlington, Virginia 22217.

Disposition

When this report is no longer needed, it may be transmitted to other authorized organizations, or properly destroyed. Do not return it to the originator or the monitoring office.

Disclaimer

The findings in this report are not to be construed as an official Department of Defense or Military Department position unless so designated by other official documents.

Reproduction

Reproduction in whole or in part is permitted for any purpose of the United States Government.

REPORT DOCUMENTATION PAGE		READ INSTRUCTIONS BEFORE COMPLETING FORM
1. REPORT NUMBER ONR-CR215-249-2F	2. GOVT ACCESSION NO.	3. RECIPIENT'S CATALOG NUMBER
4. TITLE (and Subtitle) Optimal Stochastic Path Control of Surface Ships in Shallow Water		5. TYPE OF REPORT & PERIOD COVERED Final report 1 May 76 - 30 June 77
		6. PERFORMING ORG. REPORT NUMBER No. 189
7. AUTHOR(s) Michael G. Parsons Hua Tu Cuong		8. CONTRACT OR GRANT NUMBER(s) N00014-76-C-0751
9. PERFORMING ORGANIZATION NAME AND ADDRESS Department of Naval Architecture and Marine Engr. North Campus - The University of Michigan Ann Arbor, MI. 48109		10. PROGRAM ELEMENT, PROJECT, TASK AREA & WORK UNIT NUMBERS
11. CONTROLLING OFFICE NAME AND ADDRESS Office of Naval Research, Code 211 800 North Quincy Street Arlington, VA. 22217		12. REPORT DATE 15 August 1977
		13. NUMBER OF PAGES viii + 75
14. MONITORING AGENCY NAME & ADDRESS(if different from Controlling Office)		15. SECURITY CLASS. (of this report) Unclassified
		15a. DECLASSIFICATION/DOWNGRADING SCHEDULE

16. DISTRIBUTION STATEMENT (of this Report)

Approved for public release; distribution unlimited

17. DISTRIBUTION STATEMENT (of the abstract entered in Block 20, if different from Report)

18. SUPPLEMENTARY NOTES

19. KEY WORDS (Continue on reverse side if necessary and identify by block number)

stochastic control systems   Kalman-Bucy filters
optimal control
surface ship path control
shallow water maneuvering
modern control theory

20. ABSTRACT (Continue on reverse side if necessary and identify by block number)

The control of a surface ship along a prescribed straight-line path is formulated as a stationary, linear, state-variable control problem. The open-loop characteristics of this problem are studied using data for a *Mariner* type ship at two speeds and varying water depth-to-draft ratio and for the tanker *Tokyo Maru* at one speed and varying water depth-to-draft ratio using data obtained by Fujino. Optimal stochastic control systems using a Kalman-Bucy filter and a state-feedback controller are designed for both vessels at various conditions. These designs are developed to control the ship when subject to random, zero-mean disturbances. The

DD FORM 1473   EDITION OF 1 NOV 65 IS OBSOLETE
1 JAN 73

cont: design disturbances are the yaw moment and sway force due to a passing ship which are modeled by first-order shaping filters in the design derivation. The selection of a set of measurements adequate to provide effective path control is studied. System performance is studied by the evaluation of the Root Mean Square (RMS) response of the controlled ship to the modeled design disturbances and by digital computer simulation of the response of the controlled ship to initial condition errors and the specific disturbances due to a passing ship. The effects of vessel speed and water depth on the design and performance of these controllers are studied in detail. These results yield guidance for the selection of design conditions for the design of constant-gain controllers and provide an assessment of the need for adaptive controllers which can adjust the gains to remain optimal as the ship characteristics change with vessel speed and water depth. A sensitivity study is presented to show quantitatively which of the system coefficients which change with water depth can be assumed constant and which of the coefficients must be considered variables in an adaptive path control system design.

Optimal Stochastic Path Control

of Surface Ships in Shallow Water

Michael G. Parsons
Hua Tu Cuong

ACCESSION for

NTIS   White Section ☑
DDC   B ff Section ☐
UNANNOUNCED   ☐
JUSTIFICATION _____

BY
DISTRIBUTION/AVAILABILITY CODES
Dist   SPECIAL

A

Department of Naval Architecture
and Marine Engineering
College of Engineering
The University of Michigan
Ann Arbor, Michigan 48109

Abstract

The control of a surface ship along a prescribed straight-line path is formulated as a stationary linear, state-variable control problem. The open-loop characteristics of this problem are studied using data for a *Mariner* type ship at two speeds and varying water depth-to-draft ratio and for the tanker *Tokyo Maru* at one speed and varying water depth-to-draft ratio using data obtained by Fujino. Optimal stochastic control systems using a Kalman-Bucy filter and a state-feedback controller are designed for both vessels at various conditions. These designs are developed to control the ship when subject to random, zero-mean disturbances. The design disturbances are the yaw moment and sway force due to a passing ship which are modeled by first-order shaping filters in the design derivation. The selection of a set of measurements adequate to provide effective path control is studied. System performance is studied by the evaluation of the Root Mean Square (RMS) response of the controlled ship to the modeled design disturbances and by digital computer simulation of the response of the controlled ship to initial condition errors and the specific disturbances due to a passing ship. The effects of vessel speed and water depth on the design and performance of these controllers are studied in detail. These results yield guidance for the selection of design conditions for the design of constant-gain controllers and provide an assessment of the need for adaptive controllers which can adjust the gains to remain optimal as the ship characteristics change with vessel speed and water depth. A sensitivity study is presented to show quantitatively which of the system coefficients which change with water depth can be assumed constant and which of the coefficients must be considered variables in an adaptive path control system design.

Table of Content

List of Figures

List of Tables

Nomenclature

A	state weighting matrix (nexne); helmsman transfer function gain
a	helmsman transfer function gain
B	control weighting matrix (mxm) or ship beam [m]
B_i	helmsman error function weighting factor; i=1,2,3
C	optimal control gain matrix (mxne)
E[...]	expected value or ensemble average of quantity
e	helmsman error function
F_e	estimator open-loop dynamics matrix (nexne)
$F_n=U/\sqrt{gL}$	Froude number based on ship length
F_s	system open-loop dynamics matrix (nsxns)
$F'=T^{-1}F_eT$	Jordan-form open-loop dynamics matrix (nexne)
f_{ij}	element i,j of F_e or F_s
G_e	estimator control distribution (nexm)
G_s	system control distribution matrix (nsxm)
$G'=T^{-1}G_e$	Jordan-form control distribution matrix (nexm)
G(s)	helmsman transfer function
g	acceleration of gravity [m/s^2]
H	water depth [m]
H_e	estimator measurement scaling matrix (pxne)
H_i	discrete measurement scaling matrix
H_s	system measurement scaling matrix (pxns)
$H'=H_eT$	Jordan-form measurement scaling matrix (pxne)
I_{zz}	ship yaw mass moment of inertia [kgm^2]
$I_{zz}'=2I_{zz}/\rho L^5$	nondimensional yaw mass moment of inertia
J	optimal control cost function
$\tilde{J}$	RMS cost, eq. (71)
J_{zz}	yaw added mass moment of inertia [kgm^2]
$J_{zz}'=2J_{zz}/\rho L^5$	nondimensional yaw added mass moment of inertia
j	$\sqrt{-1}$
K	Kalman-Bucy filter gain matrix (nexp); gain in Nomoto's eq(102)
K_i	discrete filter gain matrix
k_i	gains in helmsman transfer function, i=1,2,3
L	ship length between perpendiculars [m]
M_i	discrete estimate error covariance after time update
m	control vector dimension or ship mass [kg]
$m'=2m/\rho L^3$	nondimensional ship mass
m_x	surge added mass [kg]
m_y	sway added mass [kg]
$m_y'=2m_y/\rho L^3$	nondimensional sway added mass
N	total yaw moment or yaw moment disturbance [Nm]
$N'=2N/\rho L^3U^2$	nondimensional N
N_r	derivative of yaw moment w.r.t. yaw angular velocity [Nms/rad]
$N_r'=2N_r/\rho L^4U$	nondimensional N_r
N_β	derivative of yaw moment w.r.t. drift angle [Nm/rad]
$N_\beta'=2N_\beta/\rho L^3U^2$	nondimensional N_β
$N_{\dot\beta}$	derivative of yaw moment w.r.t. drift angular velocity [Nms/rad]

$N_{\dot{\beta}}'=2N_{\dot{\beta}}/\rho L^4 U$	nondimensional $N_{\dot{\beta}}$
N_δ	derivative of yaw moment w.r.t. rudder angle [Nm/rad]
$N_{\dot{\delta}}$	derivative of yaw moment w.r.t. rudder angle rate [Nms/rad]
$N_\delta'=2N_\delta/\rho L^3 U^2$	nondimensional N_δ
ne	dimension of augmented state vector
ns	dimension of state vector
P	covariance of error in estimate of augmented state $\tilde{\underline{x}}$ (nexne)
P_i	discrete filter estimate error covariance after measurement update
P_∞	steady-state value of P
p	dimension of measurement vector
Q	process disturbance power spectral density matrix (qxq)
Q_i	discrete process disturbance covariance matrix
q	dimension of disturbance vector
q_{ii}	diagnonal element i,i of Q
R	measurement noise power spectral density matrix (pxp)
R_i	discrete measurement noise covariance matrix
$r=d\psi/dt$	yaw angular velocity [rad/s]
$r'=rL/U$	nondimensional yaw angular velocity
$\dot{r}$	yaw angular acceleration [rad/s^2]
$\dot{r}'=\dot{r}L^2/U^2$	nondimensional yaw angular acceleration
r_{ii}	diagonal element i,i of R
S	solution to optimal control Riccati equation
S_∞	steady-state value of S
s	Laplace transform variable
T	modal matrix of eigenvectors of F_e; ship draft [m]; time constant in Nomoto's eq. (102)
T_L	helmsman transfer function time constant [sec]
$T_L'=T_LU/L$	nondimensional helmsman transfer function time constant
T_N	nondimensional correlation time of yaw moment disturbance; helmsman transfer function time constant [sec]
$T_N'=T_NU/L$	nondimensional helmsman transfer function time constant
T_Y	nondimensional correlation time of sway force disturbance
T_r	nondimensional rudder control time constant
t	time [s]
$t'=tU/L$	nondimensional time
U	ship speed [m/s]
u	longitudinal component of ship speed [m/s]
$\underline{u}$	control vector (mxl)
v	lateral component of ship speed [m/s]
$\underline{v}$	measurement noise vector (pxl)
$\underline{w}$	process disturbance vector (qxl)
X	surge force [N] or covariance of augmented state (nexne)
X_u	derivative of surge force w.r.t. longitudinal velocity [Ns/m]
$\hat{X}$	covariance of estimate of augmented state (nexne)
x	longitudinal axis of ship
$\underline{x}$	state vector (nsxl)
$\underline{x}'$	augmented state vector (nexl)
$\hat{\underline{x}}$	estimate of augmented state vector (nexl)
$\tilde{\underline{x}}=\hat{\underline{x}}-\underline{x}'$	error in estimate of augmented state vector (nexl)
Y	total sway force or sway force disturbance [N]
$Y'=2Y/\rho L^2 U^2$	nondimensional Y

Y_r	derivative of sway force w.r.t. yaw angular velocity [Ns/rad]
$Y_r'=2Y_r/\rho L^3 U$	nondimensional Y_r
$Y_{\dot{r}}$	derivative of sway force w.r.t. yaw angular acceleration [Ns^2/rad]
$Y_{\dot{r}}'=2Y_{\dot{r}}/\rho L^4$	nondimensional $Y_{\dot{r}}$
Y_β	derivative of sway force w.r.t. drift angle [N/rad]
$Y_\beta'=2Y_\beta/\rho L^2 U^2$	nondimensional Y_β
Y_δ	derivative of sway force w.r.t. rudder angle [N/rad]
$Y_\delta'=2Y_\delta/\rho L^2 U^2$	nondimensional Y_δ
$Y_{\dot{\delta}}$	derivative of sway force w.r.t. rudder angle rate [NS/rad]
y	transverse axis of ship
$\underline{z}$	measurement vector (px1)
$\bar{\beta}=\beta'$	drift angle [rad]
β_{ij}	angle between normal mode i and measurement j
$\dot{\beta}$	drift angular velocity [rad/s]
$\dot{\beta}'=\dot{\beta}L/U$	nondimensional drift angular velocity
Γ_e	estimator disturbance distribution matrix (nexq)
Γ_i	discrete disturbance distribution matrix
Γ_s	system disturbance distribution matrix (nsxq)
$\Gamma'=T^{-1}\Gamma_e$	Jordan-form disturbance distribution matrix (nexq)
γ_{ij}	element i, j of Γ
$\delta=\delta'$	rudder angle [rad]
$\delta_c=\delta_c'$	commanded rudder angle [rad]
$\delta(t-\tau)$	Dirac delta function
$\delta*$	desired rudder angle [rad]
η	lateral offset from nominal track [m]
$\eta'=\eta/L$	nondimensional η
Θ	eq. (25)
θ_{ij}	angle betweeen normal mode i and control j
$\Lambda=T^{-1}F_e T$	Jordan-form open-loop dynamics matrix (nexne)
λ_i	nondimensional eigenvalue i of open-loop or closed-loop system
ξ	position along nominal track [m]
$\underline{\xi}'$	Jordan-form state vector (nex1)
ρ	water density [kg/m^3]
σ	standard deviation
$\underline{\sigma}$	measurement noise standard deviation vector used to estimate R
$\underline{\sigma}'$	measurement noise standard deviation vector used in simulation
τ	dummy time variable or correlation time
Φ_i	discrete open-loop dynamics matrix
$\psi=\psi'$	heading angle [rad]
$(\underline{\ldots})$	vector quantity
$(\dot{\ldots})$	derivative w.r.t. time
$(\ldots)_\infty$	steady-state value of quantity, t=∞
$(\tilde{\ldots})$	root mean square (RMS) value of quantity (except $\tilde{J}$)
$\Delta(\ldots)$	error in quantity
$(\ldots)_o$	initial value of quantity; desired value of quantity on prescribed path; acceptable value of quantity used in forming A and B weighting matrices

1. Introduction

The problem of controlling surface ships along prescribed paths in maneuvering situations is becoming increasingly important from operational, safety, and environmental viewpoints. In these situations, the ships are subjected to short-term disturbances due to passing ships, current and wind changes, waves, and bank and bottom changes. To complicate the problem, the dynamic characteristics of surface ships change significantly with depth-under-keel and vessel speed. These maneuvering situations can place severe demands on pilots, conning officers, and helmsmen. Thus, some form of automated path control may become highly desireable or necessary in the future. An adaptive system which can automatically account for the changes in ship characteristics with changing depth and speed may be needed.

With the increasing size of ships, more meaneuvering is now performed in waters which must be considered shallow; i.e., when the ratio of water depth H to ship draft T becomes less than 3 or so and significant changes in maneuvering characteristics occur. Fujino[1,2] has shown that as ships enter shallow water they usually become less course stable as H/T approaches about 2 and then become more course stable in even shallower water. Some ships, such as the 150,000 deadweight ton tanker *Tokyo Maru* tested by Fujino, are course stable for large and small values of H/T but are unstable for some intermediate range of depth-to-draft ratio. The water depth would then be expected to have a significant effect on the design and performance of surface ship path controllers.

Most surface ship autopilots or controllers in use today are designed to provide only heading control in deep water. These are usually analog controllers which utilize various dead bands and operator adjustments to improve performance in waves, adapt for speed changes, etc. In the maneuvering situations of interest here there is a need to control along a prescribed path rather than just maintain a prescribed heading. Similar needs exist in underway replenishment and mine sweeping. In path control, the objective is to control the deviation of the ship from the prescribed path as well as the heading. A multiple-variable control problem such as this is best treated using modern, state-variable control methods. These methods are directly compatible with the use of digital computer controllers. Further, since most of the disturbances which the ship experiences are random and/or unpre-

dictable in advance it can be helpful to treat the ship motion and disturbances as stochastic processes when developing the control systems.

The theory for the optimal control of linear stochastic systems was well developed in the 1960's. Presentations by Bryson[3,4] and Gelb[5] are particularly clear and useful. Timman[6] introduced the use of optimal stochastic control systems for ship control in this country in 1972. Some investigations concerning the use of stochastic control systems for surface ship path control have recently appeared outside the United States. Zuidweg[7,8] developed an optimal, stochastic path controller for a ship subjected to random disturbances due to waves, wind, and current in deep water. Millers[9] developed an optimal, stochastic path controller for the maneuvering of a large tanker through a narrow passage involving a slight turn in the approach to Brofjorden, Sweden. We feel the use of optimal, stochastic control systems such as these offers considerable promise for improved surface ship control and safety in the future.

There have been primarily three objectives in the research which we have recently completed.

- the formulation and general characterization of the surface ship path control problem in shallow water using the state variable approach;
- the study of the feasibility and effectiveness of using optimal stochastic controllers for surface ship path control in shallow water including an evaluation of the effects of speed and depth changes on controller design and performance and an assessment of the need for adaptive systems; and
- the development and careful documentation of computer-aided tools for the design and evaluation of optimal stochastic controllers.

This paper presents the results of the first two portions of this work. Section 2 presents the derivation of the linear state-variable equations of motions for the movement of a surface ship along a straight-line path. The effect of water depth and vessel speed on the open-loop characteristics of the *Mariner* type ship and *Tokyo Maru* studied Fujino is also presented. In Section 3 we formulate the optimal stochastic control problem and present

the results for the design of a controller for the *Tokyo Maru* at one of its least course stable depth-to-draft ratios. Section 4 presents an investigation of the effect of ship speed and water depth on the design and performance of the optimal stochastic path controllers. In Section 5 we briefly discuss the digital computer simulation of stochastic controllers and present selected simulation results for the controllers we have designed for the *Tokyo Maru*. Finally, in Section 6 we present an evaluation of the need to adapt path control systems for water depth dependent changes in the various terms in the equations of motion.

The final objective of our research has been the development of computer-aided design tools. Much of our work utilized the OPTSYS program[10] which was originally developed under A.E. Bryson, Jr. at Stanford University by W.E. Hall, Jr. and extended by other Stanford students. We gratefully acknowledge Prof. Bryson for providing the version of this program which we have modified and adapted for our use under the Michigan Terminal System (MTS). This program provides very fast and efficient solutions to the steady-state, linear optimal control and filtering problems including root mean square (RMS) response evaluation and controllability and observability evaluation. The principal new tool developed in support of the work reported here is the SHIPSIM/OPTSIM program for the simulation of the response of stationary linear optimal stochastic control systems to initial condition errors and specific process disturbances while subject to measurement noise. Our separate report on SHIPSIM/OPTSIM[11] includes user's documentation, programmer's documentation and listings for this program plus user's documentation for our version of the OPTSYS program. This reference is a useful supplement to the material presented here.

2. Equations of Motion

The development of the linearized, state-variable equations of motion for a surface ship moving in the horizontal plane presented here begins with the formulation presented by Fujino[2] except that a canal wall is omitted. The coordinate system for the problem is shown in Fig. 1. The $O-\xi\eta$ system is fixed in space with the desired straight ship path along the ξ-axis. The CG-xy system is fixed at the center of gravity of the ship. The direction of the arrows define the positive sense of the drift angle β, the heading angle ψ, and the rudder angle δ. We consider here only motion in the horizontal plane and assume that roll is negligible. Thus only three coordinates x, y, and ψ need to be considered.

$$u = dx/dt$$
$$v = dy/dt$$
$$U = (u^2+v^2)^{1/2}$$
$$r = d\psi/dt$$
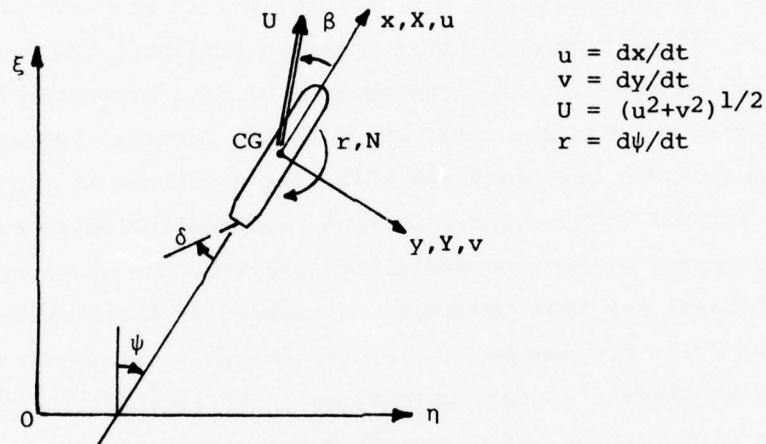
Figure 1.   Coordinate System for Path Control

The exact equations for the horizontal plane movement of a ship are integro-differential equations in which convolution integrals represent the history effect of the fluid to previous ship motion.[12,13] Alternatively, the equations can be written as differential equations in which the coefficients are frequency dependent. Recently, Fujino[14] has shown that for maneuvers of interest here the frequency dependence is negligible and constant-coefficient differential equations can be utilized. For small deviations as will be true with effective path control, the differential equations can be linearized about the nominal path by taking small perturbations from the equilibrium state and retaining only the linear terms. Applying the usual symmetry arguments, these linearized equations can be reduced to the following[2]:

-4-

$$(m+m_x)\frac{du}{dt} = X_u u, \tag{1}$$

$$(m+m_y)\frac{dv}{dt} = Y_v v + (-mU+Y_r)r + Y_{\dot{r}}\dot{r}+Y_\delta\delta+Y_{\dot{\delta}}\dot{\delta} \ , \tag{2}$$

$$(I_{zz}+J_{zz})\frac{dr}{dt} = N_v v + N_r r+N_{\dot{v}}\dot{v}+N_\delta\delta+N_{\dot{\delta}}\dot{\delta} \ , \tag{3}$$

where the derivative X_u is the partial derivative of the surge force with respect to a longitudinal velocity perturbation u with all other quantities at the equilibrium straight-line, constant speed U condition, etc. In the linearized, small perturbation equations, the longitudinal or surge equation decouples and thus need not be considered further here. Further, the terms involving $\dot{\delta}$ are small and can be neglected.

For the path control problem, we are also interested in the lateral offset or deviation from the desired path, η, which is given by the additional differential equation,

$$\frac{d\eta}{dt} = U \sin (\psi-\beta) \ , \tag{4}$$

for which the following approximation is valid for small deviations,

$$\frac{d\eta}{dt} = U \ (\psi-\beta). \tag{5}$$

It is common to utilize the drift angle instead of the lateral velocity in ship maneuvering work. These are related by,

$$v = -U \sin \beta, \tag{6}$$

for which the following approximation is valid for small deviations,

$$v = -U\beta \ . \tag{7}$$

Using eq. (7), eq. (2) and (3) can next be expressed in terms of the drift angle β ,

$$- (m+m_y)U\frac{d\beta}{dt} = Y_\beta\beta+ (-mU+Y_r)r+Y_{\dot{r}}\dot{r}+Y_\delta\delta \ , \tag{8}$$

$$(I_{zz}+J_{zz})\frac{dr}{dt} = N_\beta\beta+N_r r+N_{\dot{\beta}}\dot{\beta}+N_\delta\delta \ . \tag{9}$$

Finally, we can nondimensionalize eq. (5), (8), and (9) as indicated in the Nomenclature to yield,

$$-(m'+m_y')\frac{d\beta'}{dt'} = Y_\beta'\beta'+(-m'+Y_r')r'+Y_{\dot{r}}'\dot{r}'+Y_\delta'\delta'+Y' , \tag{10}$$

$$(I_{zz}'+J_{zz}')\frac{dr'}{dt'} = N_\beta'\beta'+N_r'r'+N_{\dot{\beta}}'\dot{\beta}'+N_\delta'\delta'+N' , \tag{11}$$

$$\frac{d\eta'}{dt'} = \psi'-\beta' , \tag{12}$$

where an external sway force disturbance Y' and yaw moment disturbance N' have been included for generality.

Equations (10) and (11) can be transformed into state-variable form by solving eq. (11) for $\dot{r}'$ and substituting this into eq. (10) and by solving eq. (10) for $\dot{\beta}'$ and substituting this into eq. (11). These can then be rearranged to yield,

$$\frac{dr'}{dt'} = f_{22}r'+f_{23}\beta'+f_{25}\delta'+\gamma_{21}N'+\gamma_{22}Y' , \tag{13}$$

$$\frac{d\beta'}{dt'} = f_{32}r'+f_{33}\beta'+f_{35}\delta'+\gamma_{31}N'+\gamma_{32}Y' , \tag{14}$$

where the coefficients f_{ij} and γ_{ij} are defined as follows:

$$f_{22} = \frac{N_r'(m'+m_y')-N_{\dot{\beta}}'(-m'+Y_r')}{\Theta} , \tag{15}$$

$$f_{23} = \frac{N_\beta'(m'+m_y')-N_{\dot{\beta}}'Y_\beta'}{\Theta} , \tag{16}$$

$$f_{25} = \frac{N_\delta'(m'+m_y')-N_{\dot{\beta}}'Y_\delta'}{\Theta} , \tag{17}$$

$$\gamma_{21} = f_{26} = \frac{(m'+m_y')}{\Theta} , \tag{18}$$

$$\gamma_{22} = f_{27} = -\frac{N_{\dot{\beta}}'}{\Theta} , \tag{19}$$

$$f_{32} = -\frac{(-m'+Y_r')(I_{zz}'+J_{zz}')+Y_{\dot{r}}'N_r'}{\Theta} , \tag{20}$$

$$f_{33} = -\frac{Y_\beta'(I_{zz}'+J_{zz}')+Y_{\dot{r}}'N_\beta'}{\Theta} , \tag{21}$$

$$f_{35} = -\frac{Y_\delta'(I_{zz}'+J_{zz}')+Y_{\dot{r}}'N_\delta'}{\Theta} , \tag{22}$$

$$\gamma_{31} = f_{36} = -\frac{Y_{\dot{r}}'}{\Theta} , \tag{23}$$

$$\gamma_{32} = f_{37} = -\frac{(I_{zz}{}'+J_{zz}{}')}{\Theta} \quad , \tag{24}$$

and where,

$$\Theta = (m'+m_y{}')(I_{zz}{}'+J_{zz}{}')+Y_{\dot{r}}{}'N_{\dot{\beta}}{}' \quad . \tag{25}$$

Now to complete the state-variable formulation we can add the definition of the yaw rate,

$$\frac{d\psi'}{dt'} = r' \ , \tag{26}$$

and represent the rudder control system by a first-order system with time constant T_r as given by the following in nondimensional form:

$$\frac{d\delta'}{dt'} = \frac{1}{T_r}(\delta_c{}'-\delta') \ , \tag{27}$$

where $\delta_c{}'$ is the commanded rudder angle. Equations (12), (13), (14), (26), and (27) can now be rewritten in vector form,

$$\frac{d}{dt'}\begin{bmatrix}\psi'\\r'\\\beta'\\\eta'\\\delta'\end{bmatrix} = \begin{bmatrix}0&1&0&0&0\\0&f_{22}&f_{23}&0&f_{25}\\0&f_{32}&f_{33}&0&f_{35}\\1&0&-1&0&0\\0&0&0&0&-1/T_r\end{bmatrix}\begin{bmatrix}\psi'\\r'\\\beta'\\\eta'\\\delta'\end{bmatrix} + \begin{bmatrix}0\\0\\0\\0\\1/T_r\end{bmatrix}\delta'_c + \begin{bmatrix}0&0\\\gamma_{21}&\gamma_{22}\\\gamma_{31}&\gamma_{32}\\0&0\\0&0\end{bmatrix}\begin{bmatrix}N\\Y\end{bmatrix}. \tag{28}$$

Equation (28) is now in state-variable form; i.e.,

$$\overset{nsx1}{\dot{\underline{x}}} = F_s\,\underline{x} + \overset{mx1}{G_s\,\underline{u}} + \overset{qx1}{\Gamma_s\underline{w}} \tag{29}$$

where the dimensions, vectors and matrices are defined by direct comparison between eq. (28) and (29). The subscript s is used on the open-loop dynamics matrix F_s, control distribution matrix G_s, and disturbance distribution matrix Γ_s to signify the system equations in contrast to the augmented state equations used below in the stochastic controller design.

At this point it is useful to present typical numerical values for the coefficients of the state equations. The principal source of maneuvering coefficients for surface ships in various water depths is the work of Fujino.[1,2] Fujino conducted planar motion mechanism (PMM) and oblique tow tests of models for a *Mariner* type ship and for the tanker *Tokyo Maru* at various water depth-to-draft ratios, H/T. Table 1 gives selected characteris-

tics of Fujino's models. The *Mariner* tests were conducted at Froude numbers corresponding to 7 and 12 knots full-scale. The *Tokyo Maru* tests were complete only for a Froude number corresponding to about 10.7 knots full-scale. (Fujino apparently quotes this speed incorrectly as 12 knots; we have assumed his Froude number to be correct.) These data were used for this study. Additional shallow water data for a *Mariner* type ship and two Series 60 hulls has been recently presented by Loeser.[15]

Fujino's data was transformed using eq. (15) through (25) and the resulting f_{ij} and γ_{ij} coefficients are given in Tables 2, 3, and 4. Table 2 presents coefficients for the *Mariner* at 7 knots full-scale and values of H/T equal to 1.21, 1.50, 1.93, 2.50, and ∞. The deep water tests were conducted at about H/T=30. Table 3 presents coefficients for the *Mariner* at 12 knots full-scale and values of H/T equal to 1.50, 1.93, 2.50, and ∞. Tests at H/T=1.21 were not feasible at this speed due to squat. Table 4 presents coefficients for the *Tokyo Maru* at 10.7 knots full-scale at values of H/T equal to 1.30, 1.50, 1.89, 2.50, and ∞. The significant variation in these coefficients with water depth and vessel speed is evident from these Tables.

	Mariner type ship	*Tokyo Maru*
linear scale ratio, λ	64.37	145.0
length between perpendiculars, mm	2,500.0	2,000.0
breadth, mm	359.8	327.6
draft fore, mm	106.5	110.3
aft, mm	125.5	110.3
mean, mm	116.0	110.3
displacement, kg	61.4	58.4
block coefficient, C_B	0.5888	0.8054
LCB, mm from amidships	39.4 aft	50.8 forward
rudder area, mm^2	-	3,390.9
propeller diameter, mm	104.2	53.8
pitch, mm	108.1	39.8
expanded area ratio	0.565	0.619
number of blades	4	5

Table 1. Characteristics of Fujino's *Mariner* and *Tokyo Maru* Models

H/T	1.21	1.50	1.93	2.50	∞
f_{22}	-4.4390	-2.6960	-2.3764	-2.1962	-2.1939
f_{23}	10.413	7.5634	5.6534	4.2852	3.3658
f_{25}	-0.96338	-1.3331	-1.4537	-1.5947	-1.4609
$\gamma_{21}=f_{26}$	712.14	822.90	909.93	963.51	971.78
$\gamma_{22}=f_{27}$	17.386	14.392	-1.8014	-4.6587	-4.4228
f_{32}	-0.58224	0.012533	0.15168	0.18097	0.28585
f_{33}	-1.5734	-0.98808	-0.80288	-0.72058	-0.89059
f_{35}	-0.26338	-0.19531	-0.23307	-0.20998	-0.20813
$\gamma_{31}=f_{36}$	75.829	30.465	23.556	23.294	13.082
$\gamma_{32}=f_{37}$	-29.013	-42.020	-50.808	-55.058	-64.162

Table 2. Coefficients of *Mariner* versus H/T at F_n=0.0905 (7 knots full-scale)

H/T	1.21	1.50	1.93	2.50	∞
f_{22}	*	-2.8841	-2.4840	-2.2777	-2.3735
f_{23}	*	12.099	6.9127	5.2893	3.9383
f_{25}	*	-1.1092	-1.4273	-1.4299	-1.4789
$\gamma_{21}=f_{26}$	*	844.31	1008.1	1042.0	1119.6
$\gamma_{22}=f_{27}$	*	37.953	-11.624	-8.0196	-4.2418
f_{32}	*	-0.018982	0.087791	0.16516	0.29637
f_{33}	*	-0.87677	-0.65628	-0.75592	-0.80577
f_{35}	*	-0.19512	-0.25534	-0.19323	-0.19941
$\gamma_{31}=f_{36}$	*	57.380	75.242	30.551	14.603
$\gamma_{32}=f_{37}$	*	-29.783	-48.715	-52.591	-62.167

*not possible due to squat

Table 3. Coefficients of *Mariner* versus H/T at F_n=0.155 (12 knots full-scale)

H/T	1.30	1.50	1.89	2.50	∞
f_{22}	-1.6508	-1.7136	-1.7657	-1.8177	-1.9515
f_{23}	9.3157	6.6235	5.7359	4.6112	3.1591
f_{25}	-0.55543	-0.79235	-0.88074	-1.0416	-1.0410
$\gamma_{21}=f_{26}$	346.69	385.98	477.68	536.00	567.13
$\gamma_{22}=f_{27}$	4.8040	-2.2145	-5.0043	-5.8625	2.3365
f_{32}	0.02974	0.13890	0.17199	0.23621	0.31507
f_{33}	-1.0388	-0.71895	-0.52766	-0.54560	-0.63651
f_{35}	-0.09995	-0.12092	-0.15607	-0.16639	-0.16163
$\gamma_{31}=f_{36}$	11.825	14.230	21.141	21.942	16.844
$\gamma_{32}=f_{37}$	-19.216	-23.123	-28.233	-31.490	-37.384

Table 4. Coefficients of *Tokyo Maru* versus H/T at F_n=0.103 (10.7 knots full-scale)

The final coefficient in eq. (28) requiring numerical definition is the nondimensional time constant of the rudder control system T_r. Typically, oceangoing ships have a maximum rudder capability of ±35° and are required to have a rudder rate capability of at least 2.33°/s. For a first-order system as assumed in eq. (27), the time constant T_r is the time at which the response to a step change in commanded rudder angle reaches $1-e^{-1}=0.632$ of its final or commanded value. With an initial rudder angle of zero and a commanded 35° rudder, it would require 9.5 seconds to reach 0.632x35=22.1° at the minimum rate. It is thus reasonable to assume a dimensional time constant of about 10 seconds as done by Millers.[9] Figure 2 illustrates this situation. The time constant of 10 seconds corresponds to a maximum rudder rate of 3.5 °/s. with a 35° command. Since the nondimensionalization used here is speed dependent, a 10 second rudder time constant becomes $T_r=0.223$ for the *Mariner* at $F_n=0.0905$ or 7 knots full-scale and $T_r=0.382$ at $F_n=0.155$ or 12 knots full-scale. A 10 second rudder time constant becomes $T_r=0.189$ for the *Tokyo Maru* at $F_n=0.103$ or 10.7 knots full-scale.
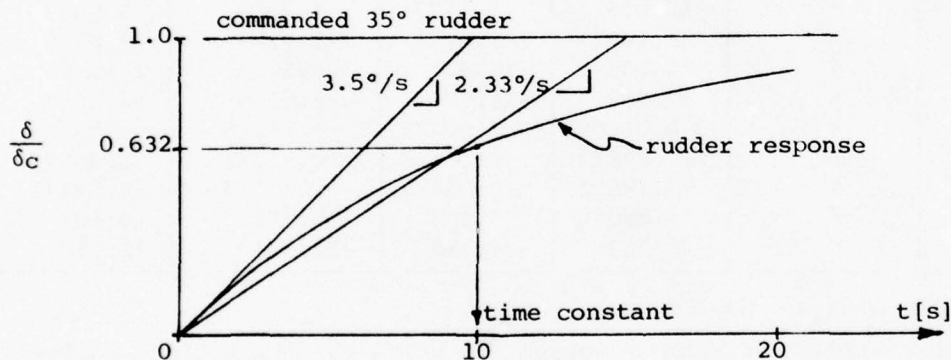
Figure 2. Response of First-order Rudder Model to 35° Step Command

With numerical values established for all terms in eq. (28) it is now possible to study the open-loop eigenvalues for the uncontrolled ship. These were found using the OPTSYS program which utilizes Wilkinson's QR algorithm to solve the open-loop eigensystem. The ship path control problem as formulated in eq. (28) has five eigenvalues. Two eigenvalues are zero and thus independent of vessel speed and water depth. A third eigenvalue is associated with the rudder control system. This eigenvalue equals $-1/T_r$ and in dimensional form is also independent of vessel speed and water depth. In the nondimensional form used here this eigenvalue appears to be vessel speed

dependent. The remaining two eigenvalues vary with both vessel speed and water depth and are of primary interest here. Table 5 presents the open-loop eigenvalues for the *Mariner* at the Froude numbers corresponding to 7 and 12 knots full-scale. The vessel is course stable under all conditions. The results for 7 knots show an initial decrease in stability as shallow water is entered (H/T=2.50) and then greatly increased stability in very shallow water (H/T$\leq$1.50). The two eigenvalues converge at about H/T=1.4 and then become a conjugate pair for lower values of H/T. Table 6 presents the open-loop eigenvalues for the *Tokyo Maru* at the Froude number corresponding to 10.7 knots full-scale. The eigenvalues are real for all H/T. The tanker is much less course stable than the *Mariner* and becomes unstable (eigenvalue with positive real part) for the intermediate range of water depth-to-draft ratio around H/T=2.50 and H/T=1.89. These results, of course, correspond to the behavior shown earlier by Fujino[1] using a different approach from the same data.

	F_n=0.0905		F_n=0.155	
$\lambda_1 = \lambda_2$	0.0		0.0	
$\lambda_3 = -1/T_r$	-4.478		-2.615	
H/T	λ_4	λ_5	λ_4	λ_5
∞	-.3646	-2.720	-.2549	-2.924
2.50	-.3095	-2.607	-.3116	-2.722
1.93	-.3745	-2.805	-.3693	-2.771
1.50	-.9343	-2.750	-.9986	-2.762
1.21	-3.006 ± 2.002j		not feasible	

Table 5. Open-loop Eigenvalues for *Mariner*

$\lambda_1 = \lambda_2$	0.0	
$\lambda_3 = -1/T_r$	-5.281	
H/T	λ_4	λ_5
∞	-.0992	-2.489
2.50	.0405	-2.404
1.89	.0237	-2.317
1.50	-.1358	-2.297
1.30	-.7360	-1.954

Table 6. Open-loop Eigenvalues for *Tokyo Maru* at F_n=0.103

The open-loop eigenvectors for the uncontrolled ship are also of interest. The repeated, zero eigenvalue has only one linearly independent eigenvector $[0,0,0,1,0]^T$; i.e., just η'. This can be viewed as the steady-motion condition where the ship has constant lateral offset; i.e. $r'=\beta'=\psi'=\delta'=0$ but $\eta'\neq0$. A second, generalized eigenvector[16] can be associated with the zero eigenvalues. This eigenvector can be shown to be $[\alpha,0,0,1,0]$ where α is any nonzero quantity. This can be viewed as the steady-motion condition where the ship has a constant heading away from the desired track; i.e., $r'=\beta'=\delta'=0$ but $\psi'\neq0$ and $\dot{\eta}'\neq0$. The remaining three eigenvectors associated with λ_3, λ_4, and λ_5 are vessel speed and water depth dependent. These eigenvectors are shown for the *Mariner* at four water depth and vessel speed conditions in Table 7 and for the *Tokyo Maru* at $F_n=0.103$ in Table 8. The eigenvector associated with λ_3 is the only one containing a δ' component as expected. This eigenvector has some water depth dependence but strong vessel speed dependence as shown in Table 7 due primarily to the improved rudder effectiveness with vessel speed. The eigenvectors associated with λ_4 and λ_5 show much smaller vessel speed dependence but a much larger water depth dependence for both types of ships. The eigenvector associated with the dominant eigenvalue λ_4 shows a major change in character as the ships become extremely course stable in very shallow water.

eigenvector associated with $\lambda_3 = -1/T_r$				
F_n	0.0905	0.155	0.0905	0.155
H/T	∞	∞	1.50	1.50
ψ' component	-0.1179	0.3300	-0.1021	-0.3138
r' component	0.5278	-0.8629	0.4571	0.8205
β' component	0.0067	0.1782	0.0477	0.0597
η' component	0.0278	-0.0581	0.0335	0.1429
δ' component	0.8406	0.3338	0.8816	0.4521

eigenvector associated with λ_4				
F_n	0.0905	0.155	0.0905	0.155
H/T	∞	∞	1.50	1.50
ψ' component	-0.2890	-0.2813	-0.5257	-0.5455
r component	0.1054	0.0556	0.4911	0.5447
β component	0.0573	0.0299	0.1144	0.0849
η component	0.9498	0.9738	0.6851	0.6313
δ' component	0.0000	0.0000	0.0000	0.0000

eigenvector associated with λ_5				
F_n	0.0905	0.155	0.0905	0.155
H/T	∞	∞	1.50	1.50
ψ' component	-0.3405	-0.3201	-0.3392	-0.3377
r' component	0.9262	0.9361	0.9329	0.9328
β' component	-0.1447	-0.1309	-0.0066	0.0094
η' component	0.0720	0.0647	0.1210	0.1256
δ' component	0.0000	0.0000	0.0000	0.0000

Table 7. Open-loop Eigenvectors for *Mariner* at Four Conditions

eigenvector associated with $\lambda_3 = -1/T_r$					
H/T	∞	2.50	1.89	1.50	1.30
ψ' component	-0.0541	-0.0496	-0.0387	-0.0341	-0.0178
r' component	0.2859	0.2621	0.2046	0.1801	0.0938
β' component	0.0139	0.0208	0.0247	0.0206	0.0228
η' component	0.0129	0.0133	0.0120	0.0104	0.0077
δ' component	0.9566	0.9635	0.9777	0.9828	0.9951
eigenvector associated with λ_4					
H/T	∞	2.50	1.89	1.50	1.30
ψ' component	-0.0933	0.0412	0.0238	-0.1304	-0.5220
r' component	0.0093	0.0017	0.0006	0.0177	0.3842
β' component	0.0054	0.0007	0.0002	0.0042	0.0377
η' component	0.9958	0.9991	0.9997	0.9913	0.7606
δ' component	0.0000	0.0000	0.0000	0.0000	0.0000
eigenvector associated with λ_5					
H/T	∞	2.50	1.89	1.50	1.30
ψ' component	-0.3669	-0.3792	-0.3913	-0.3942	-0.4450
r' component	0.9132	0.9115	0.9067	0.9053	0.8693
β' component	-0.1553	-0.1159	-0.0871	-0.0797	-0.0283
η' component	0.0850	0.1095	0.1313	0.1369	0.2133
δ' component	0.0000	0.0000	0.0000	0.0000	0.0000

Table 8.   Open-loop Eigenvectors for *Tokyo Maru* at $F_n=0.103$

3. Optimal Stochastic Path Controller Design

This section will begin with a brief introduction to the optimal control of stochastic linear systems. Readers already familiar with these ideas can continue to the second subsection.

3.1 Introduction to Optimal Stochastic Control[3,4,17]

Many physical control problems can be realistically represented using stochastic disturbances and measurement noise. This is particularly true where disturbances are of a random nature or where they cannot be defined specifically in advance. The response of a system subjected to stochastic disturbances and measurement noise can also be treated as a stochastic quantity. The engineering approach can be to model stochastic physical systems as Gauss-Markov processes. These can be represented by the state vector of a linear dynamical system forced by a gaussian purely-random process where the initial state vector is also gaussian or normally distributed. Thus we can represent the system by eq. (29) which we repeat again here for reference; i.e.,

$$\overset{ns \times 1}{\underline{\dot{x}}} = F_S \underline{x} + \overset{m \times 1}{G_S \underline{u}} + \overset{q \times 1}{\Gamma_S \underline{w}} \; . \tag{29}$$

The system open-loop dynamics matrix F_S, the system control distribution matrix G_S, and the disturbance distribution matrix Γ_S are assumed constant here. The condition of this system is completely represented by the mean value vector $\overline{\underline{x}}$ and the covariance matrix X for the ns differentiated or state variables; i.e.,

$$\overline{\underline{x}}(t) = E[\underline{x}(t)] \quad \text{with} \quad \overline{\underline{x}}(t_o) = \overline{\underline{x}}_o \; , \tag{30}$$

$$X(t) = E[(\underline{x}(t) - \overline{\underline{x}}(t))(\underline{x}(t) - \overline{\underline{x}}(t))^T] \quad \text{with} \quad X(t_o) = X_o \; , \tag{31}$$

where $E[...]$ is the expected value or ensemble average over the many possible observations at time t. The m non-differentiated variables in $\underline{u}$ are the control variables. The q variables in $\underline{w}$ are the process disturbances which are gaussian purely-random processes or white noise. White noise is an idealized, very-jittery process which can be viewed as the limit of a sequence of impulses with random magnitude and random time of occurrence. The impulses average zero over time but have an average square magnitude given by $\sigma(t)$ squared. We thus have,

$$E[\underline{w}(t)] = 0 \quad , \tag{32}$$

$$E[\underline{w}(t)\underline{w}(\tau)^T] = Q(t)\delta(t-\tau) \quad , \tag{33}$$

where Q is the power spectral density matrix which can be related to $\sigma(t)$ and $\delta(t-\tau)$ is the Dirac delta function. It is also assumed that there is no correlation between the process disturbance and the initial condition of the system; i.e.

$$E[\underline{w}(t)(\underline{x}(t_o)-\underline{\bar{x}}_o)^T] = 0 \quad . \tag{34}$$

The control problem is to develop the optimal state-variable feedback control,

$$\underline{u} = C\underline{x} \quad , \tag{35}$$

where C is the control feedback gain matrix. In general, not all of the needed states in $\underline{x}$ are readily measured. Further, it is not necessary to measure all the states if it is possible to estimate the remaining states from those which are most easily measured. In the stochastic case we may have p available measurements represented by,

$$\underset{\underline{z}}{\overset{p\times1}{\underline{z}}} = H_S\underline{x} + \underline{v} \quad , \tag{36}$$

where H_S is the measurement distribution matrix (assumed constant here) and $\underline{v}$ is a vector of white measurement noise with statistical properties,

$$E[\underline{v}(t)] = 0 \quad , \tag{37}$$

$$E[\underline{v}(t)\underline{v}(\tau)^T] = R(t)\delta(t-\tau) \quad , \tag{38}$$

$$E[\underline{v}(t)\underline{w}(\tau)^T] = E[\underline{v}(t)(\underline{x}(t_o)-\underline{\bar{x}}_o)^T] = 0 \quad . \tag{39}$$

The matrix R is the power spectral density of the measurement noise. Equation (39) states that there is no correlation between the measurement noise and the process disturbance or the initial state of system. The elements of $\underline{z}$ may be measurements of specific states or linear combinations of the states.

In modeling physical systems, it is not always realistic to assume that the process disturbance or measurement noise is white noise. If the process disturbance is a random quantity which changes very rapidly compared to the time response of the system, it is reasonable to assume the process disturbance

is white noise as in Eq. (29). However, if the process disturbance is a random quantity which changes very slowly compared to the time response of the system (perhaps a tidal current effect on a passing ship), it is reasonable to assume the process disturbance to be a random bias or constant. This can be incorporated into the above treatment by defining an additional state variable or variables such that,

$$\dot{x}_{n+1} = 0 \ , \tag{40}$$

and $x_{n+1}(t_o)$ is random. This state variable is included in an augmented state vector of length n+1 with the n+1 component from the disturbance equal to zero.

If the process disturbance is a random quantity which changes on about the same time scale as the response of the system, it must be modeled as something between white noise and a random bias. This is accomplished by the use of various shaping filters and again augmenting the state vector. The simplest shaping filter produces an exponentially correlated disturbance[3] by driving a first-order system by white noise. A new state variable is defined as follows:

$$\tau \ \dot{x}_{n+1} + x_{n+1} = w \ , \tag{41}$$

where τ is the disturbance correlation time and w is white noise. The state vector can then be augmented to an n+1 vector and the total system is still disturbed by white noise as in eq. (29). The shaping filter processes the white noise to produce a new disturbance x_{n+1} which is random but with a characteristic time constant τ of about the same order as the response time of the system. Other higher-order shaping filters are possible to model more complex disturbances.[3,5,18]

If shaping filters are used to model some ne-ns of the disturbances, the augmented state vector is then of length ne and the stochastic controller design is performed using a set of augmented or estimator-design state equations combining eq. (29) and ne-ns equations like eq. (41); i.e.,

$$\overset{\text{ne}\times 1}{\underline{\dot{x}}'} = F_e \underline{x}' + G_e \overset{\text{m}\times 1}{\underline{u}} + \Gamma_e \overset{\text{q}\times 1}{\underline{w}} \tag{42}$$

where the disturbance $\underline{w}$ is composed of only white noise with a power spectral

density given by Q. To complete the formulation, the measurement eq. (36) can now be expressed in terms of the augmented state vector to be,

$$\underline{z} = [H_s \mid 0] \underline{x}' + \underline{v} = H_e \underline{x}' + \underline{v} \quad . \tag{43}$$

The Separation Theorem[3] states that the optimal way to control the system eq. (29) which has been modeled by eq. (42) using the information available in the noisy measurements eq. (43) is to design controller gains neglecting $\underline{w}$ and $\underline{v}$ and thus assuming perfect knowledge of $\underline{x}'$. This control would be given by,

$$\underline{u} = C\underline{x}' \quad . \tag{44}$$

The noisy measurements $\underline{z}$ can then be utilized in an optimal stochastic observer (state estimator) or Kalman-Bucy filter to produce a maximum-likelihood estimate of the augmented state vector $\hat{\underline{x}}$ which includes estimates of the actual states $\underline{x}$ plus estimates of any augmented states created in the modeling. This estimated state vector is available to be used in eq. (44) so the optimal control will then be given by,

$$\underline{u} = C\hat{\underline{x}} \quad . \tag{45}$$

Thus, the controller design can be completely separated from the processing of the noisy measurements to produce the best estimate of the current state of the system. An overall schematic of such a stochastic control system is shown in Figure 3. The measurements $\underline{z}$ from the sensors are used in the optimal stochastic observer to produce an estimate of the states $\hat{\underline{x}}$ which are then used in the optimal controller to produce the control signals $\underline{u}$ given to the actuators.

An optimal control can be defined in many ways. The most common when we want to control $\underline{x}$ near zero using reasonable values of control $\underline{u}$ is to use the control which minimizes a linear quadratic cost function,

$$J = \frac{1}{2} \int_{t_o}^{t_f} (\underline{x}'^T A \underline{x}' + \underline{u}^T B \underline{u}) dt \quad , \tag{46}$$

where the A and B matrices are initially established by the designer to reflect the relative weighting of errors in the various states and the use
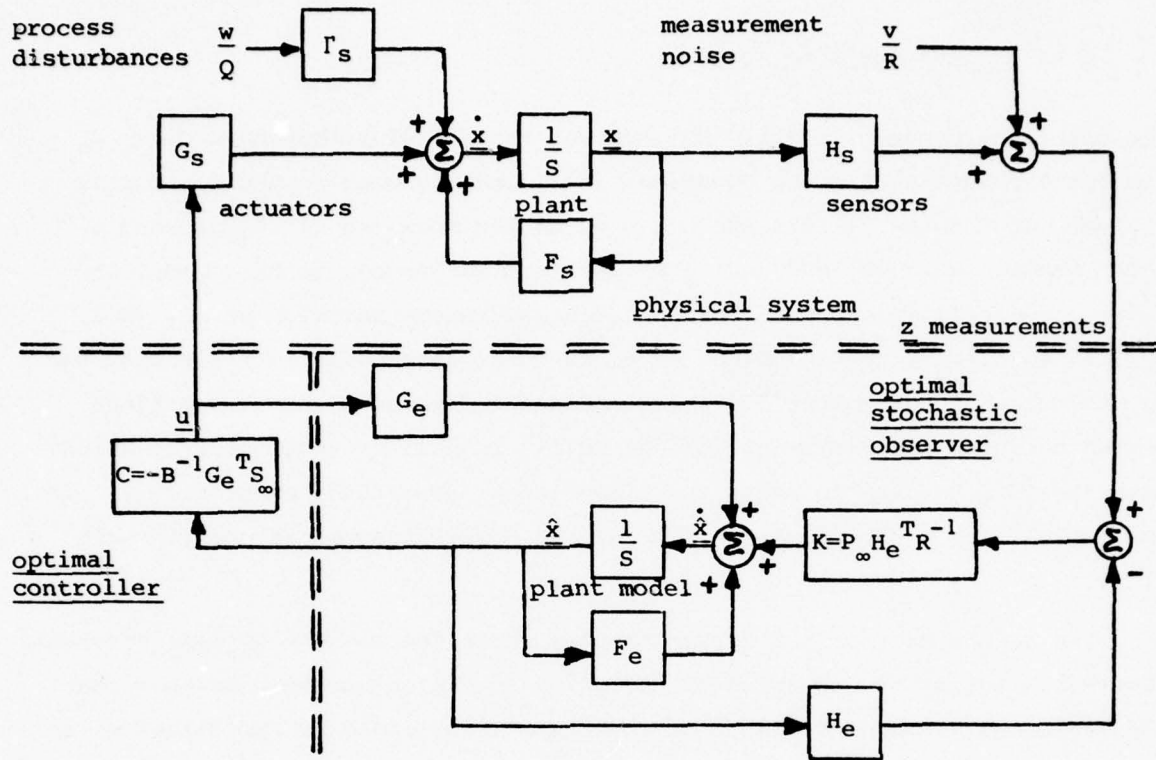
Figure 3. Overall Schematic of Optimal Stochastic Control System

of the various controls. The A and B matrices are usually diagonal with at least some nonzero diagonal elements selected to be,

$$A_{ii} = \frac{1}{x_{oi}{}^2} \quad \text{and} \quad B_{jj} = \frac{1}{u_{oj}{}^2} \quad , \tag{47}$$

where u_{oj} is an acceptable amount of control j to be used when the state i deviates x_{oi} from zero. It is usually necessary to modify the weighting matrices A and B and iterate on the design based on the evaluated response of the controlled system. The calculus of variations[3,17] can be utilized to show that the control which minimizes eq. (46) for a stationary system is given by,

$$C = -B^{-1}G_e{}^T S_\infty \quad , \tag{48}$$

where S_∞ is the steady-state solution of a matrix Riccati equation which is independent of the process disturbance $\underline{w}$ and Q and the measurement noise

$\underline{v}$ and R; i.e.,

$$\dot{S} = -SF_e - F_e^T S + SG_e B^{-1} G_e^T S - A \quad . \tag{49}$$

The open-loop dynamics matrix F_e and the control distribution matrix G_e are for the augmented state equations (42) actually used in the controller design. If shaping filters are not used in the modeling of the process disturbances, eq. (29) and (42) are identical so $ne=ns$, $F_e=F_s$, $G_e=G_s$, and $\Gamma_e=\Gamma_s$. An efficient way to obtain the steady-state solution to eq. (49), S_∞, is to utilize the technique of eigenvector decomposition first proposed by MacFarlane[19] and Potter[20]. This method was developed into a practical design computer program by Bryson and Hall[10] in Hall's OPTSYS program which uses the QR algorithm to solve the eigensystem. User's documentation is available[11] for the Michigan version of the OPTSYS program as used in this study.

The second half of the design problem is to develop the optimal stochastic observer. Again, the calculus of variations[17] can be utilized to show that the maximum-likelihood estimate of the state is produced by the filter given by,

$$\dot{\hat{\underline{x}}} = F_e\hat{\underline{x}} + G_e\underline{u} + K(\underline{z}-H_e\hat{\underline{x}}) \quad ; \quad \hat{\underline{x}}(t_o) = \overline{\underline{x}}_o \quad , \tag{50}$$

where the filter gain matrix K for a stationary system is given by,

$$K = P_\infty H_e^T R^{-1} \quad , \tag{51}$$

where P_∞ is the steady-state solution of the matrix Riccati equation,

$$\dot{P} = F_e P + PF_e^T + \Gamma_e Q\Gamma_e^T - PH_e^T R^{-1} H_e P \quad . \tag{52}$$

The matrix P is the covariance of the error of the estimate of the state; i.e.,

$$P(t) \equiv [E(\hat{\underline{x}}(t)-\underline{x}'(t))(\hat{\underline{x}}(t)-\underline{x}'(t))^T] \quad . \tag{53}$$

In eq. (50), it can be seen that the estimate $\hat{\underline{x}}$ is assumed to follow the same dynamics as $\underline{x}'$ (excluding $\Gamma\underline{w}$) and that whenever the measurement which would result from $\hat{\underline{x}}$ (excluding $\underline{v}$) deviates from the actual measurement $\underline{z}$ a correction is introduced to drive $\hat{\underline{x}}$ closer to $\underline{x}'$. In eq. (52), it can

be seen that, as expected, large process disturbances (high Q) and large measurement noise (high R) will increase P, the error in the estimate produced by the stochastic observer. An efficient way to obtain the steady-state solution to eq. (52), P_∞ , is again by eigenvector decomposition as implemented in the OPTSYS program used in this study.

Summarizing, if a physical system, its disturbances, and measurement noise are modeled as described above, a design program such as the OPTSYS program can be used to produce the optimal control gains C and the optimal filter gains K. The OPTSYS program can also produce the Root Mean Square (RMS) response of the system to the *design disturbances* as represented in the power spectral densities Q and R. The RMS response is, however, not that meaningful to many engineers. Further if specific physical disturbances were modeled in the design process using shaping filters, the designer may also want to know the response of the controlled system to the *specific disturbances*. Thus, there is often a need to simulate the response of the optimal stochastic control system to specific process disturbances and initial condition errors while subject to the measurement noise. The SHIPSIM/OPTSIM simulation program[11] which we have developed as a complement to the OPTSYS program allows the simulation of these systems with a minimum of effort and computer programming.

3.2 Process Disturbance Modeling

A ship moving along a prescribed path can be subjected to many types of short term disturbances. Waves provide a relatively high frequency disturbance. Changes in current, banks, and bottom can also provide significant disturbances. For this study, we selected as the design disturbance the yaw moment and sway force due to a passing ship which constitute one of the strongest disturbances a ship can experience in maneuvering situations. Data given by Newton[21] was utilized to establish a representative magnitude and time history for this disturbance. His particular data were for a *Mariner* moving in deep water. Yung[22] and Abkowitz, Ashe, and Fortson[23] show a significant increase in the disturbance yaw moment and sway force due to a passing ship as water depth decreases so Newton's data is clearly lower than would be expected in shallow water. For the purposes of this study, we wanted only a representative disturbance so the yaw moment and sway force design disturbances shown in

Fig. 4 were chosen and assumed to be independent of ship type, and water depth, and vessel speed.

N'x10^5 Y'x10^5

Ships beam-to-beam at t'=0
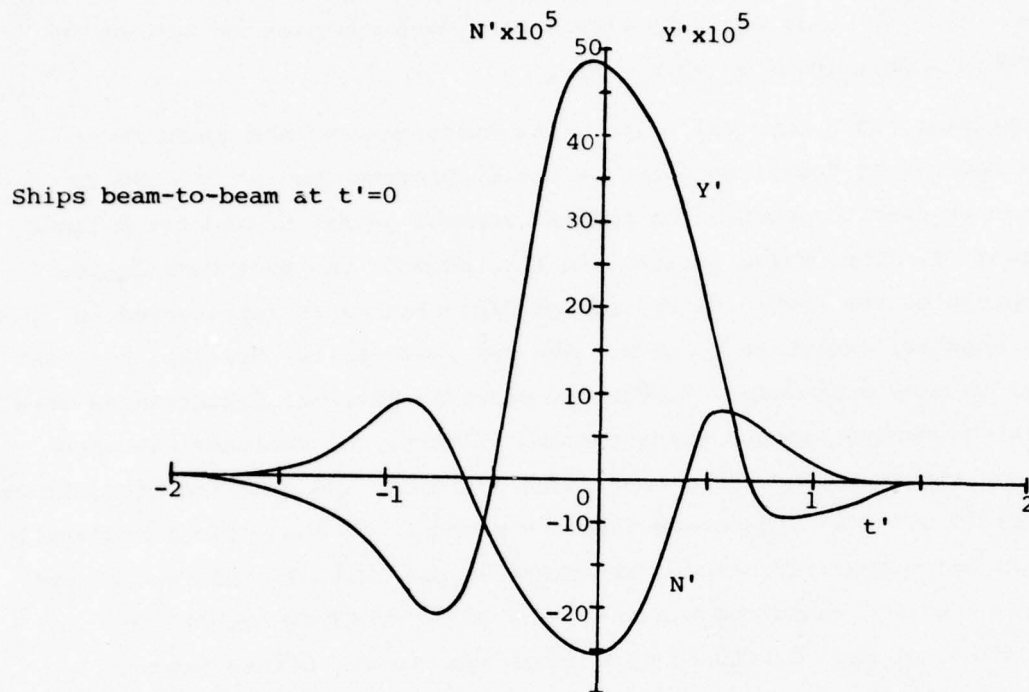
Figure 4. Design Yaw Moment and Sway Force Disturbances due to
Passing Ship

Disturbances as assumed in Fig. 4 can be reasonably modeled as exponentially correlated disturbances as produced by first-order shaping filters driven by white noise. Thus, two new states were defined by,

$$T_N\frac{dN'}{dt'} = -N' + w_N \quad , \tag{54}$$

$$T_Y\frac{dY'}{dt'} = -Y' + w_Y \quad , \tag{55}$$

where the correlation times were taken as $T_N=T_Y=1$ or dimensionally the time it takes the ship to travel its own length. The power spectral densities for the white noise w_N and w_Y were defined based on the Root Mean Square (RMS) values of N' and Y', respectively, during the t' period $(-2,+1.5)$ shown on Fig. 4; i.e., $\tilde{N}'=0.880\times10^{-4}$ and $\tilde{Y}'=2.118\times10^{-4}$. The white noise power spectral densities are then given by[3],

$$q_{11} \cong 2(\tilde{N}')^2 T_N = 1.548\times10^{-8} \quad , \tag{56}$$

for w_N and,

$$q_{22} \cong 2(\tilde{Y}')^2 T_Y = 8.970 \times 10^{-8} \quad , \tag{57}$$

for w_Y. The *design disturbances* are fully defined by q_{11}, q_{22}, $q_{12}=q_{21}=0$, and eq. (54) and (55). Simulation of the controlled ship subjected to the *specific disturbances* shown in Fig. 4 have confirmed the validity of this modeling approach as will be discussed below.

With two shaping filters used to model the yaw moment and sway force disturbances, the augmented system eq. (42) used in the stochastic control system design combine eq (28), (54), and (55) to give,

$$\frac{d}{dt'} \begin{bmatrix} \psi' \\ r' \\ \beta' \\ \eta' \\ \delta' \\ N' \\ Y' \end{bmatrix} = \begin{bmatrix} 0 & 1 & 0 & 0 & 0 & 0 & 0 \\ 0 & f_{22} & f_{23} & 0 & f_{25} & f_{26} & f_{27} \\ 0 & f_{32} & f_{33} & 0 & f_{35} & f_{36} & f_{37} \\ 1 & 0 & -1 & 0 & 0 & 0 & 0 \\ 0 & 0 & 0 & 0 & -1/T_r & 0 & 0 \\ 0 & 0 & 0 & 0 & 0 & -1/T_N & 0 \\ 0 & 0 & 0 & 0 & 0 & 0 & -1/T_Y \end{bmatrix} \begin{bmatrix} \psi' \\ \beta' \\ r' \\ \eta' \\ \delta' \\ N' \\ Y' \end{bmatrix} + \begin{bmatrix} 0 \\ 0 \\ 0 \\ 0 \\ 1/T_r \\ 0 \\ 0 \end{bmatrix} \delta_c' + \begin{bmatrix} 0 & 0 \\ 0 & 0 \\ 0 & 0 \\ 0 & 0 \\ 0 & 0 \\ 1/T_N & 0 \\ 0 & 1/T_Y \end{bmatrix} \begin{bmatrix} w_N \\ w_Y \end{bmatrix} . \tag{58}$$

The dimensions, vectors, and matrices of eq. (42) are defined by direct comparison with eq. (58). Notice that the upper right (5x2) partition of F_e in eq. (58) is Γ_s in eq. (28); i.e. $f_{26}=\gamma_{21}$, $\gamma_{36}=\gamma_{31}$, etc.

3.3 Selection of Measurements

The measurements eq. (43) and associated measurement noise power spectral density matrix R were established next. In this study, we considered the use of a ψ' measurement from a compass or gyro compass, an r' measurement from a rate gyro, a $\beta'=-v'$ measurement from a doppler sonar, and an η' measurement from radar or DECCA. Rudder angle could be easily obtained but was not considered here. The first consideration to answer in selecting measurements is whether or not all the states of the path control problem are observable with a given measurement or set of measurements $\underline{z}$. If a state is not observable with a given $\underline{z}$, it is impossible to design a filter which can produce the augmented state vector estimate $\hat{\underline{x}}$ from the measurement vector $\underline{z}$.

One way to establish the observability of eq. (42) and eq. (43) is through the use of a Jordan-form transformation[16]. If the open-loop eigenvectors of

F_e are grouped together as columns of a transformation matrix T, the problem can be transformed into its equivalent Jordan-form using the transformation $\underline{\xi}'=T^{-1}\underline{x}$. Using this transformation eq. (42) and (43) become,

$$\dot{\underline{\xi}}' = \Lambda\underline{\xi} + G'\underline{u} + \Gamma'\underline{w} \quad , \tag{59}$$

and,

$$\underline{z} = H'\underline{\xi} + v \quad , \tag{60}$$

where,

$$\Lambda = T^{-1}F_eT \quad , \tag{61}$$

$$G' = T^{-1}G_e \quad , \tag{62}$$

$$\Gamma' = T^{-1}\Gamma_e \quad , \tag{63}$$

$$H' = H_eT \quad .$$

In this form, the various modes of response of the system are completely decoupled provided the eigenvalues of F_e are distinct. In that case, matrix Λ is a diagonal matrix with the open-loop eigenvalues of F_e down the diagonal. The structure of H' can be studied to quickly establish the observability of each mode of the system with each measurement in $\underline{z}$. Similarly, the structure of G' can be studied to establish the controllability of each mode of the system with each component of the control vector $\underline{u}$.

The ship path control problem as formulated in eq. (58) has seven eigenvalues, two of which are zero, but only six independent eigenvectors. The Jordan-form transformation can be performed using these six eigenvectors plus an additional, generalized eigenvector $[\alpha\ 0\ 0\ 1\ 0\ 0\ 0]^T$, $\alpha>0$ as discussed in Section 2. Four of the eigenvectors are identical to those presented in Section 2 with two zeros added to make them of dimension (7x1). Two additional eigenvectors are associated with the shaping filters. The essential elements of the resulting Jordan-form structure are shown in Fig. 5 where ξ_2' is associated with the generalized eigenvector for the repeated eigenvalue $\lambda_1=\lambda_2=0$. The OPTSYS program was utilized to perform the Jordan-form transformation and to establish numerical values for matrices G', H', and Γ'. If H_{j1}' is zero it shows directly that mode ξ_1' is not observable with measurement j, etc. Likewise, if G_{31}' is zero it directly shows that mode ξ_3' cannot be controlled with the single control δ_c' , etc.
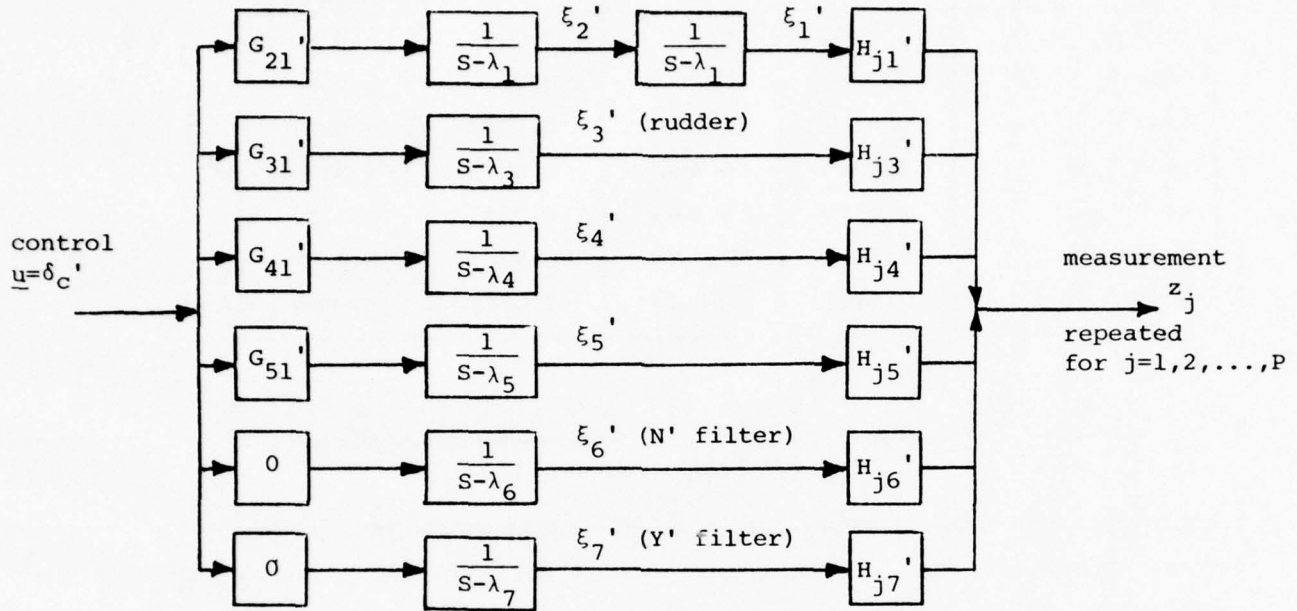
Figure 5. *Simplified Jordan-Form Structure of Path Control Problem*

The OPTSYS program also presents the elements of H' in a normalized manner based on the orthogonality between the eigenvector of T associated with mode i and the row of H associated with measurement j. A result $\cos\beta_{ij}=1$ indicates that mode i is fully observable with measurement j; a result $\cos\beta_{ij}=0$ indicates that mode i cannot be observed (or estimated) based on measurement j. The numerical value between 0 and 1 thus indicates quantitatively how observable each mode is with any particular measurement. The observability results for the *Tokyo Maru* at $H/T=1.89$ and $F_n=0.103$ are shown in Table 9. This shows that mode ξ_1' is only observable with a measurement of η' so as a minimum η' must be measured. A measurement of η' also gives good information on modes ξ_2' and ξ_3' and will allow estimation of the sway force disturbance represented in mode ξ_7'. The observability of the other modes with η' is much weaker so at least one more measurement is probably necessary. Adding an **r'** measurement gives good observability of modes ξ_4', ξ_5' and the yaw moment disturbance represented in mode ξ_6'. Thus, measurement of r' and η' would probably be sufficient. In our study, we have used measurements of ψ', r', and η' as the base set of

measurements	ψ'	r'	β'	η'
mode ξ_1'	0.0000	0.0000	0.0000	1.0000
mode ξ_2'	$f(\alpha)\neq 0$	0.0000	0.0000	1.0000
mode ξ_3'	0.0238	0.0005	0.0002	0.9997
mode ξ_4'	0.3913	0.9067	0.0872	0.1313
mode ξ_5'	0.0388	0.2046	0.0247	0.0120
mode $\xi_6'(N')$	0.5881	0.5881	0.5542	0.0339
mode $\xi_7'(Y')$	0.5487	0.5487	0.0773	0.6260

Table 9.   Observability $\cos\beta_{ij}$ of *Tokyo Maru* Modes with
Various Measurements

measurements but Table 9 shows that the ψ' measurement could probably be
omitted to simplify the control system without serious loss of controller
performance.   Table 9 also shows that the use of a doppler sonar to produce
a drift angle measurement β' could probably not be justified.

Using the measurements of ψ', r', and η' eq. (43) becomes,

$$\underline{z} = \begin{bmatrix} 1 & 0 & 0 & 0 & 0 & 0 & 0 \\ 0 & 1 & 0 & 0 & 0 & 0 & 0 \\ 0 & 0 & 0 & 1 & 0 & 0 & 0 \end{bmatrix} \underline{x}' + \underline{v} \ . \tag{65}$$

The measurement noise power spectral density matrix R for the vector $\underline{v}$ can
be estimated for each measurement by assuming an RMS noise value σ_j and a
correlation time τ_j (much faster than time constants of the ship).   The
white noise power spectral density component for measurement is then given by,[3]

$$r_{jj} \cong 2(\sigma_j)^2 \tau_j \ . \tag{66}$$

The numerical values for the noise power spectral densities of the four
possible measurements used in this study are summarized in Table 10.   In the
nondimensional form shown in Table 10 the resulting power spectral densities
r_{jj} are different for each ship and speed.   Data σ_j and τ_j for the
measurements of ψ', r', and η' are from Millers.[9]   Data for the doppler
sonar are estimated based on information for the Furuno MF-100DS.[24]   Using
measurements of ψ', r', and η' as in eq. (65), the matrix R is diagonal
with associated diagonal elements taken from Table 10.

measurement	source	σ_j	τ_j	r_{jj}		
				Mariner F_n=0.0905	*Mariner* F_n=0.155	*Tokyo Maru* F_n=0.103
ψ'	gyro compass	0.2°	0.1s.	5.441×10^{-8}	9.320×10^{-8}	4.612×10^{-8}
r'	rate gyro	0.01°/s	0.1s.	2.728×10^{-7}	1.593×10^{-7}	3.218×10^{-7}
β'	doppler sonar	0.05m/s	0.1s.	8.629×10^{-7}	5.007×10^{-7}	3.139×10^{-7}
η'	radar	10m	0.1s.	1.725×10^{-5}	2.955×10^{-5}	4.502×10^{-6}

Table 10. Measurement Noise Power Spectral Densities

The ship path control problem as formulated in eq. (58) is known to be controllable with the rudder. The G' matrix established for this problem using the OPTSYS program verifies this by having nonzero elements G_{21}', G_{31}', G_{41}', and G_{51}' which indicate that all the real states of the system can be controlled using the rudder command δ_c'. As shown in Fig. 5, elements G_{61}' and G_{71}' are zero indicating, again as expected, that the rudder command δ_c' has no influence on the yaw moment and sway force disturbances represented in mode ξ_6' and mode ξ_7', respectively.

3.4 Design Results for the *Tokyo Maru* at H/T=1.89

The example results to be presented in this section are for the *Tokyo Maru* at F_n=0.103 and H/T=1.89. As will be shown in the next section, if the stochastic path control system is to be designed for ship characteristics at a single depth it is best to choose one of the depths at which the vessel is least course stable. The *Tokyo Maru* is course unstable in the approximate range $1.75 \leq H/T \leq 2.75$ so a design depth of H/T=1.89 was selected for the base case to be presented here. The system is fully defined by eq. (58), eq. (65), and the various data presented above. The only remaining requirement is to establish the state weighting matrix A and the control weighting matrix B used in eq. (46) to define the basis for determining the optimal control gains C.

For the ship path control problem, we want to control η' and ψ' near zero without using excessive amounts of control δ_c' and thus also δ'. For

this study, we assumed that we would be willing to commit 5° rudder usage
for path control when the ship heading deviates 5° or the ship reaches a
lateral offset η_O of 10.43m for the *Tokyo Maru* or 5.79m for the *Mariner*.
This lateral offset is exactly a quarter beam (B/4) for the *Mariner* and
slightly less than a quarter beam for the *Tokyo Maru*. A 5° heading deviation
for either ship will cause the ends of the ship to be about the same
distance from the desired track as the assumed η_O value (12.7m for
Tokyo Maru; 7.0m for *Mariner*). Using eq. (47), the A and B matrices were
taken as zero except for the following elements:

$$A_{11} = (5/57.3)^{-2} = 131.332 \text{ for } \psi' , \tag{67}$$

$$A_{44} = (10.43/290)^{-2} = 772.463 \text{ for } \eta', \tag{68}$$

$$A_{55} = (5/57.3)^{-2} = 131.332 \text{ for } \delta' , \tag{69}$$

$$B = B_{11} = (5/57.3)^{-2} = 131.332 \text{ for } \delta_c' . \tag{70}$$

These A and B matrices were used for all *Tokyo Maru* and *Mariner* designs
presented here. These state deviation and control weighting terms can be
modified at the designer's discretion based on the performance of the
controlled system. Increasing the value of a term in the A matrix will
produce a system design which will more closely control the associated
state at the expense of increased deviation of the other states and the use
of more control. Increasing the value of B will reduce the amount of commanded
rudder (and also δ') at the expense of greater deviations in the other
states. For the purposes of the study presented here, the A and B matrices
were held constant (following preliminary investigations) to provide
meaningful comparisons among competing designs.

Using one control δ_c' to control five states simultaneously, it is
difficult to directly compare the RMS response of the ship to the design
disturbances when using various control systems. We have therefore used
an additional control measure-of-merit which we call the RMS cost $\tilde{J}$. This
quantity is based on eq. (46) and reflects the weighting implied by eq.
(67) through eq. (70). The RMS cost is defined by,

$$\tilde{J} = \tilde{\psi}'^2 + (A_{44}\tilde{\eta}'^2 + A_{55}\tilde{\delta}'^2 + B_{11}\tilde{\delta}_c'^2)/A_{11} , \tag{71}$$

where $(.\tilde{.}.)$ indicates the RMS value of the particular quantity. This RMS

cost $\tilde{J}$ is just twice the cost J defined by eq. (46) divided by A_{11}. For the numerical values used here this becomes,

$$\tilde{J} = \tilde{\psi}'^2 + 5.8818\tilde{\eta}'^2 + \tilde{\delta}'^2 + \tilde{\delta}_c'^2 \quad . \tag{72}$$

The cost J or $\tilde{J}$ provides the most meaningful single quantity with which to compare the RMS response of a ship when controlled by two different control systems which were developed using the same state and control weighting matrices.

Using eq. (58), eq. (65), and the A and B weighting matrices defined above, the OPTSYS program was used to determine the optimal control gains C and the optimal filter gains K for the *Tokyo Maru* at $F_n=0.103$ and H/T= 1.89. The resulting gains are as follows:

$$C^T = \begin{bmatrix} 5.6470 \\ 2.6848 \\ 6.3147 \\ 2.4252 \\ -0.8079 \\ 675.14 \\ -50.154 \end{bmatrix}; \quad K = \begin{bmatrix} 2.6321 & 0.9164 & 0.0015 \\ 6.3936 & 12.2380 & -0.0724 \\ 1.4384 & 3.2622 & -1.2160 \\ 0.1447 & -1.0125 & 1.5367 \\ 0.0000 & 0.0000 & 0.0000 \\ 0.0263 & 0.1673 & 0.0130 \\ -0.0287 & -0.1710 & 0.0319 \end{bmatrix} .$$

Notice that the estimates of the yaw force disturbance $\hat{N}'$ and the sway force disturbance $\hat{Y}'$ produced by the filter are included in the augmented state feedback; i.e., $C_{16} \neq 0$, $C_{17} \neq 0$. Also notice that the Kalman-Bucy filter does nothing (fifth row of K is zero) to improve the existing estimate of the rudder angle δ'. This is because δ' is not measured and its response depends only on the current δ' and the commanded rudder δ_c' independent of the disturbances $\underline{w}$.

The RMS response of the *Tokyo Maru* at $F_n=0.103$ and H/T=1.89 to the modeled design disturbances using measurements of ψ', r', and η' and the above control and filter gains is shown in the middle column of Table 11. The RMS cost established using eq. (72) is also shown. Dimensionally this response is $\tilde{\psi}=0.43°$, $\tilde{\eta}=3.55m$, and $\tilde{\delta}=2.6°$. The optimal stochastic control system is therefore very effective in controlling the ship when subjected to the modeled design disturbances. Notice that by properly processing the three available measurements the controller can control $\tilde{\eta}$ to 3.55m even though the RMS error in the η measurement is 10m. Also shown in Table 11 are the

RMS responses of the *Tokyo Maru* to the modeled design disturbance when controlled
by optimal stochastic controllers designed using the same A and B matrices but
one measurement η' or four measurements (ψ',r',β',η'). As expected from
the discussion above concerning   observability, control based on an η'
measurement alone is very ineffective; i.e., η̃=20m. Also, the addition of a
β' measurement produces very little improvement in controller effectiveness.

measurements	η' only	ψ', r', η'	ψ', r', β', η'
$\tilde{\psi}'$	0.04643	0.00755	0.00756
$\tilde{r}'$	0.05145	0.00876	0.00876
$\tilde{\beta}'$	0.01436	0.00501	0.00502
$\tilde{\eta}'$	0.06921	0.01223	0.01211
$\tilde{\delta}'$	0.11841	0.04521	0.04500
$\tilde{\delta}_c'$	0.14275	0.05180	0.05154
$\tilde{J}$	0.06473	0.00566	0.00560

Table 11. RMS Response of *Tokyo Maru* to Design Disturbance
using Various Measurements

A brief look at the eigenvalues associated with the optimal stochastic
controller for the *Tokyo Maru* at F_n=0.103 and H/T=1.89 is of value at this
point. Table 12 shows the open-loop eigenvalues for the ship in this
condition as presented in Section 2. The dominant eigenvalue λ_4=0.0237
indicates that the ship is course unstable. Table 12 also shows the closed-
loop eigenvalues for the ship controlled with the optimal control gains C
presented above. The optimal controller design guarantees a stable controlled
ship which is verified by these results. The dominant poles have a real
part of -0.5538 which indicates good course stability. For the Kalman-Bucy
filter to be effective in processing the noisy measurements to produce the
state estimate $\hat{x}$ it is necessary that the error in this estimate have
dynamics which are faster than the ship. If this is true, the filter will
produce an acceptable estimate $\hat{x}$ quickly enough after some change that it
can be used effectively to control the ship. The estimate error eigenvalues
are shown in Table 12 and the dominant eigenvalues indicate that the filter
will respond about twice as fast as the ship. This should prove acceptable
as will be confirmed by computer simulation results presented below.

open-loop	closed-loop	estimate error
0.0	-.5538± .8669 j	-.9111± 1.157 j
0.0		
0.0237	-0.9534	-1.824
-2.317	-2.311	-2.638
-5.281	-7.470	-5.281
-1.000 $\begin{pmatrix} \text{shaping} \\ \text{filters} \end{pmatrix}$	-1.000 $\begin{pmatrix} \text{shaping} \\ \text{filters} \end{pmatrix}$	-7.208± 7.274 j
-1.000	-1.000	

Table 12.   Eigenvalues for Optimal Design for *Tokyo Maru*

The optimal stochastic path controllers as developed here provide effective path control provided sufficient measurements, such as ψ', r', and η', are utilized.   In the following sections, we study the effect of the changes in ship characteristics due to changing water depth and ship speed on the design and performance of these controllers.   The response of these controllers to initial condition errors and the specific disturbances shown in Fig. 4 as obtained by computer simulation will also be presented.

4. Effects of Speed and Water Depth on Controller Design and Performance

As shown in Section 2, the characteristics f_{ij} and γ_{ij} for a surface ship change considerably as vessel speed and water depth change. The purpose of this section is to establish how these changes affect the design of the optimal stochastic path controllers and more importantly how these changes affect the performance of the optimal stochastic path controllers. These results help establish which speed and depth conditions should be used in design if constant control and filter gain matrices are to be utilized. These results can also indicate whether or not an adaptive path control system is necessary. Three measurements ψ', r', and η' are used throughout this section.

4.1 *Tokyo Maru* Controller Design and Performance

The shallow water data presented by Fugino[1,2] for the *Tokyo Maru* is only complete for the single Froude number $F_n=0.103$. Therefore, we could only evaluate the effect of water depth on the design and performance of the *Tokyo Maru* controllers. The versatility of the OPTSYS program allows a very meaningful study to be conducted. As presented in Section 3 for $H/T=1.89$, the optimal controller gain matrix C and the optimal Kalman-Bucy filter gain matrix K can be established for any water depth and the RMS response of the controlled ship to the modeled design disturbances can be evaluated. It is also possible to establish the RMS response of the controlled ship at any water depth using a specified set of gain matrices. This allows an evaluation of the performance of a controller designed for one water depth when operating at another water depth.

Optimal stochastic path controllers were designed for the *Tokyo Maru* for the five depth-to-draft ratios for which specific data were presented in Section 2. Table 13 gives the optimal control gains as a function of H/T. The gain on η', C_{14}, is constant with respect to H/T which could simplify implementation of an adaptive system. Two of the gains C_{13} on β' and C_{17} on Y' show major changes in value as water depth changes. Gain C_{16} on N' shows a somewhat smaller change. Gains C_{11}, C_{12}, and C_{15} show relatively small changes. Table 14 gives the optimal Kalman-Bucy filter gains for the three water depths $H/T=\infty$, $H/T=1.89$, and $H/T=1.30$. The gains $K_{51}=K_{52}=K_{53}=0$ for all depths as noted in Section 3 for $H/T=1.89$. In

-32-

general, the optimal filter gains change less with water depth than do the optimal control gains. Some gains such as K_{11} and K_{12} change very little; others such as K_{41} change by as much as a factor of three. The most important aspect, however, is not how much the gains should change with water depth to remain optimal but how much operating at an incorrect water depth affects the control performance.

H/T	1.30	1.50	1.89	2.50	∞
C_{11}	5.605	5.566	5.647	5.659	5.984
C_{12}	2.632	2.722	2.685	2.561	2.489
C_{13}	10.985	7.630	6.315	3.998	1.887
C_{14}	2.425	2.425	2.425	2.425	2.425
C_{15}	-0.723	-0.779	-0.808	-0.806	-0.760
C_{16}	547.1	563.0	675.1	693.7	731.6
C_{17}	-79.25	-56.05	-50.15	-26.29	7.033

Table 13.   Optimal Control Gains for *Tokyo Maru* versus H/T

The important considerations of how water depth affects controller performance and what water depth should be used in a constant-gain controller design can be addressed by studying Tables 15, 16, and 17. In these three Tables we present the RMS response of optimal stochastic controllers designed for the *Tokyo Maru* at H/T=∞, H/T=1.89, and H/T=1.30 when the ship is subjected to the modeled design disturbances at these same three depths. Table 15 shows the RMS response and RMS cost $\tilde{J}$ when the ship is operating at H/T=∞ using controllers which were designed to be optimal at H/T=1.30, H/T=1.89, and the existing H/T=∞. Based on RMS cost, which is the best single criterion, the design for H/T=∞ is superior as expected. The optimal design for H/T=1.89 shows an RMS cost increase from the optimal of 0.00681 to 0.00783 or 15 per cent. The RMS lateral offset $\tilde{\eta}$ increases from 4.7 m to 6.5 m. The optimal design for H/T=1.30 shows a larger RMS cost increase to 0.01056 with an RMS lateral offset increase to 8.95 m. Table 16 shows the RMS response with the same three control systems when the ship is operating at H/T=1.89. The middle column for the optimal design is a repeat of the results given in

optimal filter gains K for H/T=∞		
2.6319	0.9158	0.0013
6.3892	13.0320	-0.0594
1.5709	2.9049	-1.9634
0.1245	-0.8312	1.9697
0.0000	0.0000	0.0000
0.0294	0.1840	0.0093
-0.0180	-0.1026	0.0421
optimal filter gains K for H/T=1.89		
2.6321	0.9164	0.0015
6.3936	12.2380	-0.0724
1.4384	3.2622	-1.2160
0.1447	-1.0125	1.5367
0.0000	0.0000	0.0000
0.0263	0.1673	0.0130
-0.0287	-0.1710	0.0319
optimal filter gains K for H/T=1.30		
2.6252	0.8906	0.0037
6.2137	10.2795	-0.0476
0.8253	1.9779	-0.4600
0.3619	-0.6658	0.9457
0.0000	0.0000	0.0000
0.0324	0.1587	0.0105
-0.0406	-0.1815	0.0245

Table 14. Optimal Filter Gains for *Tokyo Maru* versus H/T

Section 3. The optimal design for H/T=∞ shows a decrease in the RMS lateral offset $\tilde{\eta}'$ with increased $\tilde{\psi}'$ and increased rudder usage. Since manipulation of the A and B matrices can alter the relative magnitudes of these values, this illustrates the need to utilize a single, rational basis upon which to compare the various designs. Based on the RMS cost, the design for H/T=∞ shows an increase from the optimal 0.00566 to 0.00644. The design for H/T=1.30 shows a smaller increase to 0.00611 with an increase in $\tilde{\eta}'$ but decreased $\tilde{\psi}'$ and decreased rudder usage. Table 17 shows the RMS response of the three control systems when the ship is operating at H/T=1.30. The design for H/T=1.89 shows a much smaller degredation in RMS cost at this shallower depth than does the design for H/T=∞. Both designs show improved RMS lateral offset $\tilde{\eta}'$ but increased $\tilde{\psi}'$ and increased rudder usage.

	Design for H/T=1.30	Design for H/T=1.89	Optimal Design
$\tilde{\psi}'$	0.00936	0.00850	0.00965
$\tilde{r}'$	0.00749	0.00753	0.00982
$\tilde{\beta}'$	0.00718	0.00756	0.00834
$\tilde{\eta}'$	0.03087	0.02238	0.01607
$\tilde{\delta}'$	0.04548	0.04533	0.04773
$\tilde{\delta}_c'$	0.05288	0.05249	0.05406
$\tilde{J}$	0.01056(+55%)	0.00783(+15%)	0.00681

Table 15. RMS Response of *Tokyo Maru* Operating at H/T=∞

	Design for H/T=1.30	Optimal Design	Design for H/T=∞
$\tilde{\psi}'$	0.00675	0.00755	0.00989
$\tilde{r}'$	0.00751	0.00876	0.01266
$\tilde{\beta}'$	0.00469	0.00501	0.00571
$\tilde{\eta}'$	0.01577	0.01223	0.01033
$\tilde{\delta}'$	0.04445	0.04521	0.05035
$\tilde{\delta}_c'$	0.05124	0.05180	0.05639
$\tilde{J}$	0.00618(+8%)	0.00566	0.00644(+14%)

Table 16. RMS Response of *Tokyo Maru* Operating at H/T=1.89

	Optimal Design	Design for H/T=1.89	Design for H/T=∞
$\tilde{\psi}'$	0.00697	0.00790	0.00904
$\tilde{r}'$	0.00830	0.00970	0.01228
$\tilde{\beta}'$	0.00234	0.00248	0.00274
$\tilde{\eta}'$	0.01133	0.01083	0.00984
$\tilde{\delta}'$	0.04318	0.04459	0.05017
$\tilde{\delta}_c'$	0.04850	0.05003	0.05562
$\tilde{J}$	0.00502	0.00524 (+4%)	0.00626 (+25%)

Table 17. RMS Response of *Tokyo Maru* Operating at H/T=1.30

A study of the results presented in Tables 15, 16, and 17 points the way
to a choice of design water depth if a constant-gain stochastic control system
is to be utilized. We conclude that if the design is to be optimal at a
single water depth, it should be designed to be optimal at an intermediate
water depth where the ship is least course stable. For the *Tokyo Maru*, the
design which is optimal at H/T=1.89 provides the best overall performance.
All three controllers are stable in all three conditions but the design for
H/T=1.89 is developed to be optimal when the ship is most difficult to
control and this seems to provide the best performance over the range of
water depths. For ships of this type, however, we feel that the results of
Tables 15, 16, and 17 show the justification for the development of an adaptive
system which could automatically adjust the C and K gain matrices to be
optimal at any operating H/T.

4.2 *Mariner* Controller Design and Performance

The *Mariner* is course stable in all water depths so the effect of water
depth on the controller design and performance could be expected to be less
than shown above for the tanker *Tokyo Maru*. Since Fujino's data for the *Mariner*
included two speeds, we conducted a study to see how both vessel speed and
water depth affected controller design and performance for this type of ship.
This was begun by developing optimal designs for the *Mariner* at the four combina-
tions of Froude numbers 0.0905 (7 knots full-scale) and 0.155 (12 knots full-
scale) and water depth-to-draft ratios H/T=∞ and H/T=1.50. Table 18 gives the

resulting optimal control gains for the four conditions. The results are similar to those shown in Table 13 for the *Tokyo Maru*. The gain on η', C_{14}, is a constant 2.425 for all conditions and thus appears independent of ship type, vessel speed, and depth-to-draft ratio. Gains C_{13} on β' and C_{17} on r' show a strong dependence on both speed and H/T. Gain C_{15} shows a larger speed dependence than depth-to-draft ratio dependence; gain C_{12} shows the opposite behavior.

F_n	0.0905	0.155	0.0905	0.155
H/T	1.50	1.50	∞	∞
C_{11}	4.997	5.203	5.361	5.658
C_{12}	1.525	1.471	1.955	2.042
C_{13}	4.039	8.077	1.170	2.020
C_{14}	2.425	2.425	2.425	2.425
C_{15}	-0.806	-1.110	-0.840	-1.149
C_{16}	698.8	861.8	947.5	1176.1
C_{17}	-41.013	-62.744	8.960	-10.976

Table 18. Optimal Control Gains for *Mariner* at Four Conditions.

Table 19 gives the optimal Kalman-Bucy filter gains for the *Mariner* in the four water depth and vessel speed conditions studied. As with the *Tokyo Maru* the optimal filter gains show relatively less variation with depth-to-draft ratio than do the optimal control gains. There appears to be a greater vessel speed dependence in the optimal filter gains but the conclusion varies from term to term as can be seen by study of Table 19.

To study the effects of vessel speed and water depth on the performance of the optimal stochastic controller for the *Mariner*, we used the design for F_n=0.155 and H/T=∞ as the base design. This was the least course stable condition for this ship as shown by the open-loop eigenvalues given in Table 5. The RMS response of the ship to the modeled design disturbances while using this control system design was then established at F_n=0.155 and H/T= 1.50, at F_n=0.0905 and H/T=∞, and at F_n=0.0905 and H/T=1.50. Table 20 gives

optimal filter gains K for F_n=0.155 H/T=∞		
1.3069	0.9836	0.0008
1.6806	23.3700	-0.0118
0.5647	5.9375	-1.0798
0.2459	-2.1920	1.4612
0.0000	0.0000	0.0000
0.0029	0.2727	0.0036
-0.0035	-0.1745	0.0133
optimal filter gains K for F_n=0.0905 H/T=∞		
2.2369	0.9559	0.0007
4.7926	18.5577	-0.0218
1.1006	4.2767	-1.4516
0.2114	-1.3801	1.6954
0.0000	0.0000	0.0000
0.0138	0.2061	0.0047
-0.0100	-0.1269	0.0199
optimal filter gains K for F_n=0.155 H/T=1.50		
1.3066	0.9780	0.0016
1.6711	20.2666	-0.0065
0.2712	4.1025	-0.2179
0.5045	-1.2028	0.6561
0.0000	0.0000	0.0000
0.0037	0.2632	0.0026
-0.0049	-0.1894	0.0083
optimal filter gains K for F_n=0.0905 H/T=1.50		
2.2357	0.9451	0.0010
4.7386	16.7166	-0.0206
0.7675	3.8652	-0.6359
0.3313	-1.3004	1.1166
0.0000	0.0000	0.0000
0.0160	0.1947	0.0051
-0.0155	-0.1648	0.0149

Table 19. Optimal Filter Gains for *Mariner* at Four Conditions

the RMS response of the base design at F_n=0.155 and the two depths H/T=∞ and
H/T=1.50. The response with the optimal design for the shallower depth is
also shown for comparison. The RMS response at H/T=∞ is $\tilde{\psi}$=92°, $\tilde{\eta}$=4.1m., and
$\tilde{\delta}$=3.64° which is comparable to the *Tokyo Maru* response even though our constant
design disturbance appears relatively larger to the *Mariner*. At the shallower
water depth the base design shows a decreased RMS lateral offset $\tilde{\eta}'$ but
increased $\tilde{\psi}'$ and increased rudder usage compared to the optimal as was

Operating H/T	1.50	1.50	∞
Design F_n Condition H/T	Optimal Design	0.155 ∞	Optimal Design
$\tilde{\psi}'$	0.01104	0.01241	0.01606
$\tilde{r}'$	0.01531	0.01920	0.01835
$\tilde{\beta}'$	0.00421	0.00479	0.01271
$\tilde{\eta}'$	0.01643	0.01239	0.02566
$\tilde{\delta}'$	0.05078	0.05838	0.06356
$\tilde{\delta}_c'$	0.06549	0.07822	0.08263
$\tilde{J}$	0.00858	0.01058(+23%)	0.01500

Table 20.   RMS Response of *Mariner* Operating at F_n=0.155

Operating H/T	1.50	1.50	∞	∞
Design F_n Condition H/T	Optimal Design	0.155 ∞	Optimal Design	0.155 ∞
$\tilde{\psi}'$	0.00910	0.00850	0.01366	0.01243
$\tilde{r}'$	0.01194	0.01155	0.01504	0.01276
$\tilde{\beta}'$	0.00557	0.00564	0.01184	0.01144
$\tilde{\eta}'$	0.01422	0.01032	0.02142	0.02245
$\tilde{\delta}'$	0.04636	0.04963	0.05717	0.05551
$\tilde{\delta}_c'$	0.05340	0.06255	0.06667	0.06837
$\tilde{J}$	0.00627	0.00707(+13%)	0.01060	0.01087(+2.5%)

Table 21.   RMS Response of *Mariner* Operating at F_n=0.0905

shown with the *Tokyo Maru*. The RMS cost increases 23% compared to the optimal.
Table 21 gives the RMS response of the base design when the ship is subjected
to the modeled design disturbances while operating at F_n=0.0905 and water
depths H/T=∞ and H/T=1.50. The RMS response of the ship with the optimal
control system design is shown in both conditions for comparison. The change
in speed in deep water shows only a small 2.5 per cent degredation in RMS

cost compared to the optimum. The RMS lateral offset $\tilde{\eta}'$ decreases but $\tilde{\psi}'$ and rudder usage increase. Notice that these effects of slowing down are opposite to the effects of entering shallow water. This apparently explains why the degredation in RMS cost compared to the optimum is less at slow speed in shallow water, F_n=0.0905 and H/T≈1.50, than at the control system design speed F_n=0.155 in the same depth water.

In general, the performance of a constant-gain stochastic control system for the *Mariner* shows a smaller loss of performance as vessel speed and water depth change than shown for the *Tokyo Maru* as water depth changes. An adaptive system might still be justified but the dimensional response is good for all vessel speeds and water depths; i.e., the worst case gives $\tilde{\eta}$=4.1m., $\tilde{\psi}$=.92°, and $\tilde{\delta}$=3.64°. A constant-gain design should be a very effective controller for a ship such as the *Mariner* which is course stable under all conditions.

5. Simulation of Optimal Stochastic Path Controllers

This section presents a general discussion of the digital computer simulation of optimal stochastic path controllers. We also present simulation results for the controller designs developed above for the *Tokyo Maru*. These results are used to evaluate the validity of using first-order shaping filters to model the yawing moment and sway force disturbances in the controller design. The section closes with a comparison of the effectiveness of the optimal controller designed for the *Tokyo Maru* at $H/T=\infty$ with the control which might be provided by a human helmsman.

The *OPTSYS* optimal stochastic controller design program can evaluate the RMS response of the controlled system to the design stochastic disturbances represented by the power spectral density Q while using measurements which are contaminated by noise represented by the power spectral density R. These RMS results are very useful in evaluating the designs but often they are difficult for designers to fully interpret. To more completely show system effectiveness there is also a need to simulate the response of the controlled system to initial condition (start-up) errors and specific process disturbances while the controller is receiving measurements containing randomly generated noise. To perform the simulations needed as part of this work, we developed the SHIPSIM/OPTSIM simulation program for stationary, linear, optimal stochastic control systems.[11] This program uses the same data sets used with or produced by the OPTSYS program so the two companion programs provide a valuable capability for the efficient design and evaluation of these controllers.

5.1 Formulation of Simulation Equations

The physical system being controlled is represented by the system equations (29); i.e.,

$$\dot{\underline{x}} = F_s\underline{x} + G_s\underline{u} + \Gamma_s\underline{w} \quad , \quad \underline{x}(t_o) = \underline{x}_o \quad , \tag{73}$$

and the measurement equation (36),

$$\underline{z} = H_s\underline{x} + \underline{v} \quad . \tag{74}$$

The optimal stochastic controller design is actually based on the augmented or estimator-design state equations (42); i.e.,

$$\underline{\dot{x}}' = H_e \underline{x}' + G_e \underline{u} + \Gamma_e \underline{w} \quad , \tag{75}$$

whenever shaping filters are used to model the process disturbances. If shaping filters are not used $\underline{x}'=\underline{x}$, $F_e=F_s$, $G_e=G_s$, and $\Gamma_e=\Gamma_s$; i.e., eq. (73) and eq. (75) are identical. The optimal stochastic controller design produces the optimal control law eq. (45); i.e.,

$$\underline{u} = C\underline{\hat{x}} \quad , \tag{76}$$

and the Kalman-Bucy filter given by eq. (50),

$$\underline{\dot{\hat{x}}} = F_e\underline{\hat{x}} + G_e\underline{u} + K(\underline{z}-H_e\underline{\hat{x}}) \quad , \qquad \underline{\hat{x}}(t_o)=\underline{\hat{x}}_o \quad . \tag{77}$$

Substituting eq. (74) and eq. (76) into eq. (73) and eq. (77) produces the state and state estimate equations which must be simulated,

$$\underline{\dot{x}} = F_s\underline{x} + G_sC\underline{\hat{x}} + \Gamma_s\underline{w} \quad , \qquad\qquad \underline{x}(t_o)=\underline{x}_o \quad , \tag{78}$$

$$\underline{\dot{\hat{x}}} = F_e\underline{\hat{x}} + G_eC\underline{\hat{x}} +KH_s\underline{x} + K\underline{v}-KH_e\underline{\hat{x}} \quad , \qquad \underline{\hat{x}}(t_o)=\underline{\hat{x}}_o \quad . \tag{79}$$

Equations (78) and (79) combine to give the (ns+ne) system of coupled first-order differential equations which the SHIPSIM/OPTSIM program simulates; i.e.,

(ns+ne)x1 $\qquad\qquad\qquad\qquad\qquad$ (q+p)x1

$$\frac{d}{dt'}\begin{bmatrix} \underline{x} \\ \underline{\hat{x}} \end{bmatrix} = \begin{bmatrix} F_s & G_sC \\ KH_s & F_e+G_eC-KH_e \end{bmatrix}\begin{bmatrix} \underline{x} \\ \underline{\hat{x}} \end{bmatrix} + \begin{bmatrix} \Gamma_s & 0 \\ 0 & K \end{bmatrix}\begin{bmatrix} \underline{w} \\ \underline{v} \end{bmatrix} \quad . \tag{80}$$

These equations are integrated by SHIPSIM/OPTSIM from a user-specified initial condition,

$$\begin{bmatrix} \underline{x}(t_o) \\ \underline{\hat{x}}(t_o) \end{bmatrix} = \begin{bmatrix} \underline{x}_o \\ \underline{\hat{x}}_o \end{bmatrix} \quad , \tag{81}$$

using any process disturbance vector $\underline{w}(t)$ produced by a user-supplied process disturbance subroutine. The zero-mean, gaussian measurement noise vector $\underline{v}(t)$ is randomly generated in accordance with a user-specified standard deviation $\underline{\sigma}'$. SHIPSIM/OPTSIM can also integrate additional differential equations and calculate any non-integrated quantities desired as part of the printed or plotted output. User's Documentation, Programmer's Documentation, and a listing for the SHIPSIM/OPTSIM program have been published separately.[11]

5.2 Selection of Integration Method and Noise Modeling

For a proper simulation of eq. (80), the selection of the integration method and the treatment of the measurement noise must be performed with care to ensure that the correct stochastic response is achieved. The most direct approach is to utilize a fixed step-size Euler or rectangular integration scheme. This has the effect of approximating the continuous Gauss-Markov process eq. (80) by a discrete Gauss-Markov sequence. In developing the design of the optimal control system, eq. (66) was used to establish the measurement noise power spectral densities. The noise was first assumed to be exponentially correlated with an RMS magnitude σ_j and a correlation time τ_j which is much faster than the time constants for the ship. Equation (66); i.e.,

$$r_{jj} \stackrel{\sim}{=} 2(\sigma_j{}^2)\tau_j \ , \tag{82}$$

was then used to calculate the magnitude of the noise power spectral density. This was then assumed constant when the noise was approximated as white noise. The RMS magnitude σ_j used in eq. (82) is not, however, the correct standard deviation component $\sigma_j{}'$ to use in the simulation of the system using Euler integration.

The use of a fixed step-size Euler integration has the effect of approximating the continuous Gauss-Markov process eq. (73) and eq. (74) by the discrete Gauss-Markov process given by,

$$\underline{x}_{i+1} = \Phi_i \underline{x}_i + \Gamma_i \underline{w}_i \ , \qquad\qquad i=0,1,\ldots,N \tag{83}$$

$$\underline{z}_i = H_i \underline{x}_i + \underline{v}_i \ , \qquad\qquad i=0,1,\ldots,N \tag{84}$$

$$E[\underline{w}_i \underline{w}_j{}^T] = Q_i \delta_{ij} \ , \tag{85}$$

$$E[\underline{v}_i \underline{v}_j{}^T] = R_i \delta_{ij} \ , \tag{86}$$

$$E[\underline{w}_i \underline{v}_j{}^T] = E[\underline{w}_i (\underline{x}_o - \underline{\bar{x}}_o)^T] = E[v_i (\underline{x}_o - \underline{\bar{x}}_o)^T] = 0 \ , \tag{87}$$

where Q_i and R_i are now covariance matrices and δ_{ij} is the Kronecker delta function. The control can be omitted in this discussion without loss of generality. If we take P_i as the error covariance of the discrete Kalman filter estimate at point i, the covariance can be propagated to the next measurement point i+1 using a time update to give the error covariance

prior to the measurements M_{i+1} and then the measurements can be processed in the measurement update to give P_{i+1}. Governing update equations can be expressed as,

$$M_{i+1} = \Phi_i P_i \Phi_i^T + \Gamma_i Q_i \Gamma_i^T \qquad \text{(time update)} , \qquad (88)$$

$$P_{i+1} = M_{i+1} - K_{i+1} H_{i+1} M_{i+1} \qquad \text{(measurement update)} , \qquad (89)$$

where,

$$K_i = P_i H_i R_i^{-1} = M_i H_i^T (H_i M_i H_i^T + R_i)^{-1} . \qquad (90)$$

When Euler integration is used with an integration step-size Δt, $\underline{x}(t+\Delta t)$ is approximated using eq. (73) to be,

$$\underline{x}(t+\Delta t) = \underline{x}(t) + F_S \underline{x}(t)\Delta t + \Gamma_S \underline{w}(t)\Delta t , \qquad (91)$$

where again the control is omitted for the purposes of this discussion. The error covariance equation (52) is not included in the simulation but the use of Euler integration has the *effect* of approximating the error covariance $P(t+\Delta t)$ as,

$$P(t+\Delta t) = P(t) + FP(t)\Delta t + P(t)F^T\Delta t + \Gamma Q\Gamma^T\Delta t - K(t)HP(t)\Delta t , \qquad (92)$$

where the filter gain matrix is given by,

$$K = P(t)H^T R^{-1} . \qquad (93)$$

For a simulation to be valid it is necessary that the discrete error covariance given by eq. (88), (89), and (90) be the same at the end of each integration step as the continuous error covariance given by eq. (92) and (93). We show in ref. 11 that this is true if the disturbance and noise covariance matrices in eq. (85) and (86) are related to the continuous system power spectral density matrices as used in the system design by,

$$Q_i \Delta t = Q , \qquad (94)$$

and

$$R_i \Delta t = R . \qquad (95)$$

The correct measurement noise covariance R_i to use in a simulation thus depends on the integration step-size Δt. If σ_j' is the standard deviation for noise element j (square root of diagonal element j of R_i which is

constant), a correct simulation must utilize,

$$\sigma_j' = \left[\frac{r_{jj}}{\Delta t}\right]^{1/2} = \left[\frac{2\sigma_j^2 \tau_j}{\Delta t}\right]^{1/2} \quad , \tag{96}$$

with the integration performed by Euler integration using a fixed step-size Δt. SHIPSIM/OPTSIM uses a fixed step-size Euler integration and in our simulations, eq. (96) was used to relate the noise standard deviation vector $\underline{\sigma}'$ to the design measurement noise level represented by the power spectral density R. A non-dimensional step-size of $\Delta t=0.005$ was found to be satisfactory for most of these simulations.

5.3 Simulation Results for *Tokyo Maru* at H/T=1.89

The SHIPSIM/OPTSIM program was used to perform a number of simulations of the *Tokyo Maru* controlled by the optimal controllers we have developed. Some of the results for the *Tokyo Maru* operating at a water depth-to-draft ratio H/T=1.89 are presented here to further illustrate the effectiveness of these controllers. Recall that the controllers we have studied are for stationary systems; i.e., the statistics of the disturbance and measurement noise (R and Q) and the various system matrices are assumed constant. The resulting control feedback gains and Kalman-Bucy filter gains are also constant.

An important question with a stationary, constant-gain control system is how the controlled system will respond if the controller is first turned on while an initial condition error exists. We simulated the start-up response of the *Tokyo Maru* controlled by the optimal stochastic controller designed for the existing depth H/T=1.89 as presented in Section 3. All initial states were taken as zero except the lateral offset η_o which was taken as one half breadth B/2 (23.75 m. full-scale). The filter has no prior knowledge at start-up so the estimate of all the states $\underline{\hat{x}}$ was taken as zero. This corresponds to the situation where the ship is just entering the restricted path area and is on a path parallel to but offset B/2 to starboard ($\eta>0$) of the prescribed path when the controller is turned on. The lateral offset response and rudder angle response are shown in Fig. 6 and Fig. 7, respectively. The lateral offset is unchanged for about one ship length while the filter generates an estimate of the initial lateral offset error, the rudder responds

to a commanded turn to port, and then the ship responds. The ship crosses the prescribed path after four ship lengths (t'=4.0) and then overshoots only about 3.2 m. before settling onto the prescribed path. The small oscillations about the path after about t'=10 are due primarily to the measurement noise which is present throughout the simulation. The excellent startup response with the optimal controller is clearly shown by Fig. 6. The maximum rudder usage shown on Fig. 7 is dimensionally about 3.4°. The continuing rudder movement due to the measurement noise after about t'=10 has peak values of only about 1° and while this would be undesirable for steering system wear reasons in continuous operation it should be very acceptable for short-term operations in restricted waters.
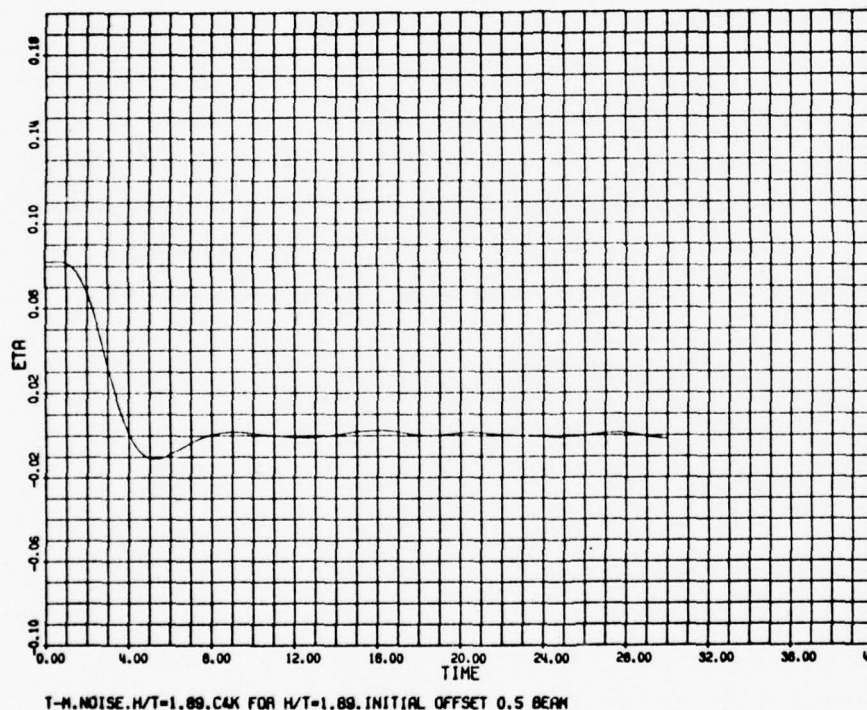

T-M.NOISE.H/T=1.89.C4K FOR H/T=1.89.INITIAL OFFSET 0.5 BEAM

Figure 6. Lateral Offset Response to B/2 Initial Offset: Optimal Control

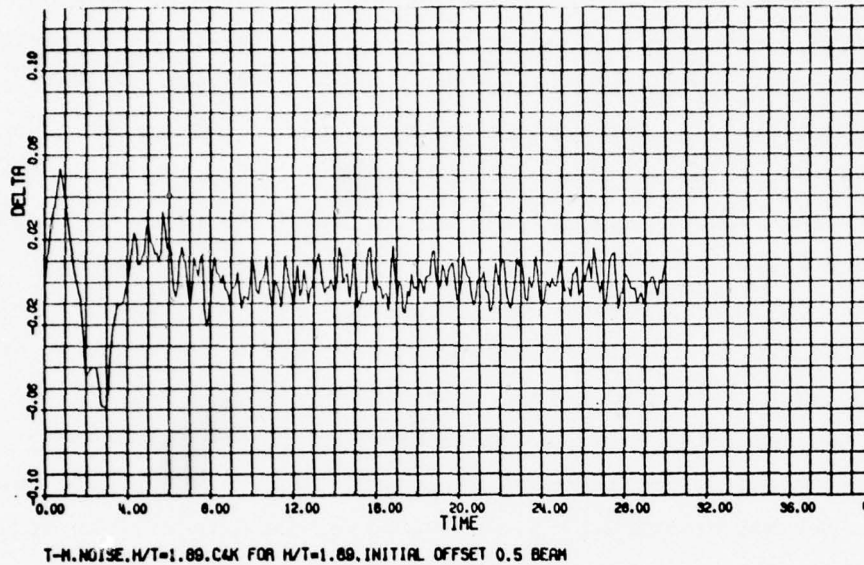T-M.NOISE.H/T=1.89.C4K FOR H/T=1.89.INITIAL OFFSET 0.5 BEAM

Figure 7.   Rudder Angle Response to B/2 Initial Offset: Optimal Control

The design process disturbance used to develop the optimal controllers was based on the yaw moment and sway force due to a passing ship as shown in Fig. 4.   These disturbances were modeled by two first-order shaping filters as described in Section 3.   Since it is of interest to see how the optimally controlled system would respond to the actual yaw moment and sway force disturbances shown in Fig. 4, the *Tokyo Maru* with the optimal controller was next simulated to pass the ship respresented by these disturbances.   The simulation was begun with no initial error; i.e., $\underline{x}=\hat{\underline{x}}=0$, and the two ships were simulated to passed beam-to-beam at t'=7.   Simulation results are shown in Fig. 8, 9, and 10.   Figure 8 shows the lateral offset response of the *Tokyo Maru*.   The maximum response is only about 1.7m. which occurs at about t'=8.5 or one ship length after the ship has passed.   This response is low for two reasons.   First, the disturbances shown in Fig. 4 are relatively small for a ship the size of the *Tokyo Maru*.   Secondly, the optimal control system is very effective in controlling the ship.   While response to the measurement noise after t'=18 appears large due to the plot scaling, it has a peak value of only about 0.6 m.   The maximum response due to the passing ship would increase roughly linearly with the disturbance magnitude if the

passing ship were larger or closer or if the effect of shallow water were to increase the disturbance magnitude significantly as discussed in Section 3.2. The disturbance magnitudes shown in Fig. 4, are, therefore, completely valid for linear control system design and evaluation. The rudder angle response is shown in Fig. 9. The maximum rudder angle of about 6.9° occurs just a few seconds after the maximum disturbance at $t'=7$ when the ships are passing beam-to-beam. The estimate of the yaw moment disturbance $\hat{N}$ produced by the Kalman-Bucy filter is shown in Fig. 10. Notice that the maximum value of -19.4×10^{-5} at $t'=7$ compares very favorably with the peak value of -20.0×10^{-5} shown on Fig. 4. This peak value also occurs when the ships are beam-to-beam or $t'=7$ in this simulation. The estimate of the sway force disturbance $\hat{Y}$ is less effective. The effectiveness of the Kalman-Bucy filter to process the noisy measurements of ψ', r', and η' to produce good estimates of the yaw moment and sway force acting on the ship will be studied further below.
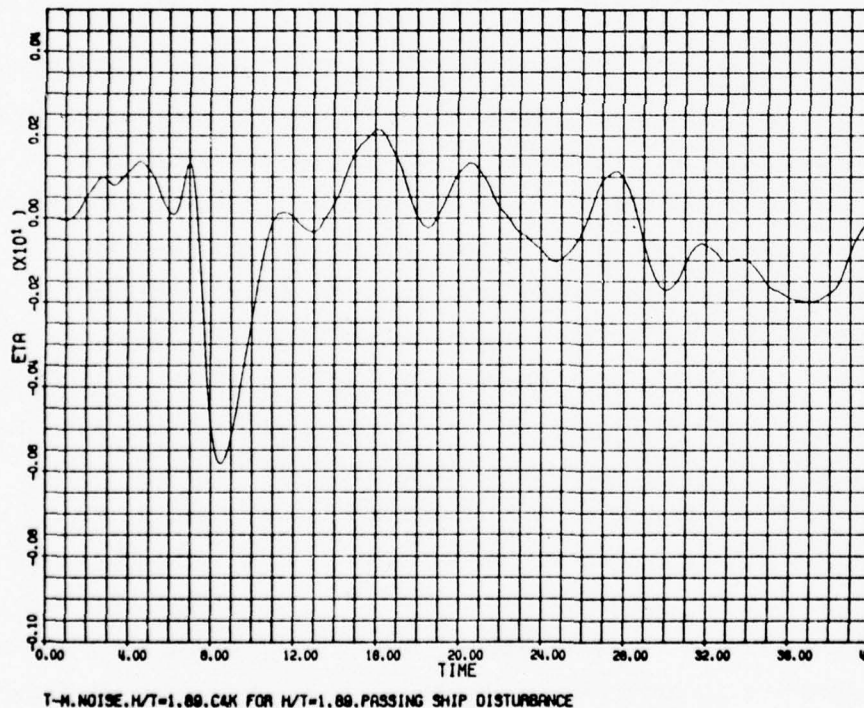

T-M.NOISE.H/T=1.89.C4K FOR H/T=1.89.PASSING SHIP DISTURBANCE

Figure 8. Lateral Offset Response to Passing Ship: Optimal Control

-49-

T-M.NOISE.H/T=1.69.C4K FOR H/T=1.69.PASSING SHIP DISTURBANCE
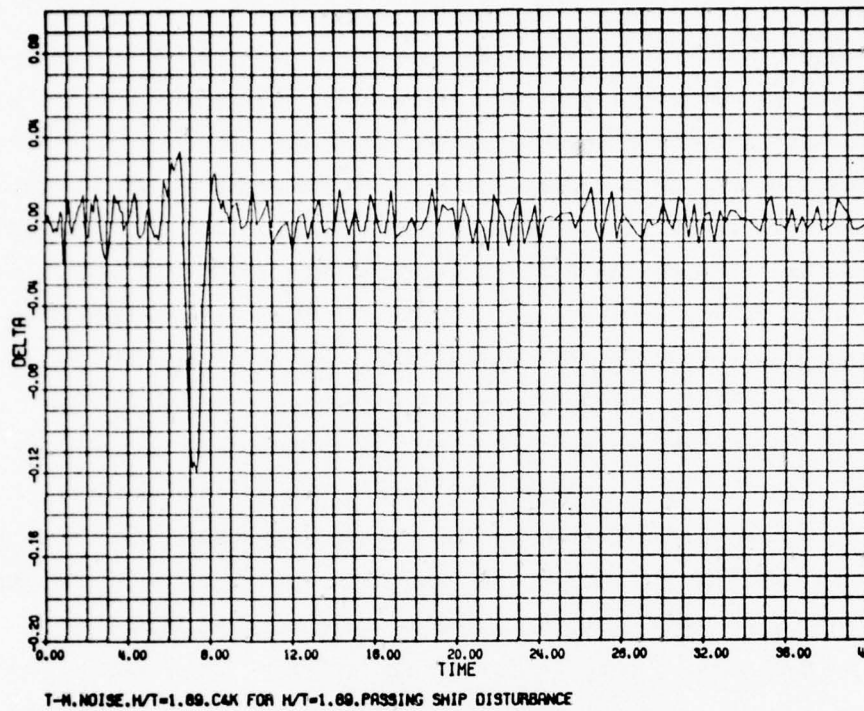
Figure 9.   Rudder Angle Response to Passing Ship: Optimal Control

T-M.NOISE.H/T=1.69.C4K FOR H/T=1.69.PASSING SHIP DISTURBANCE
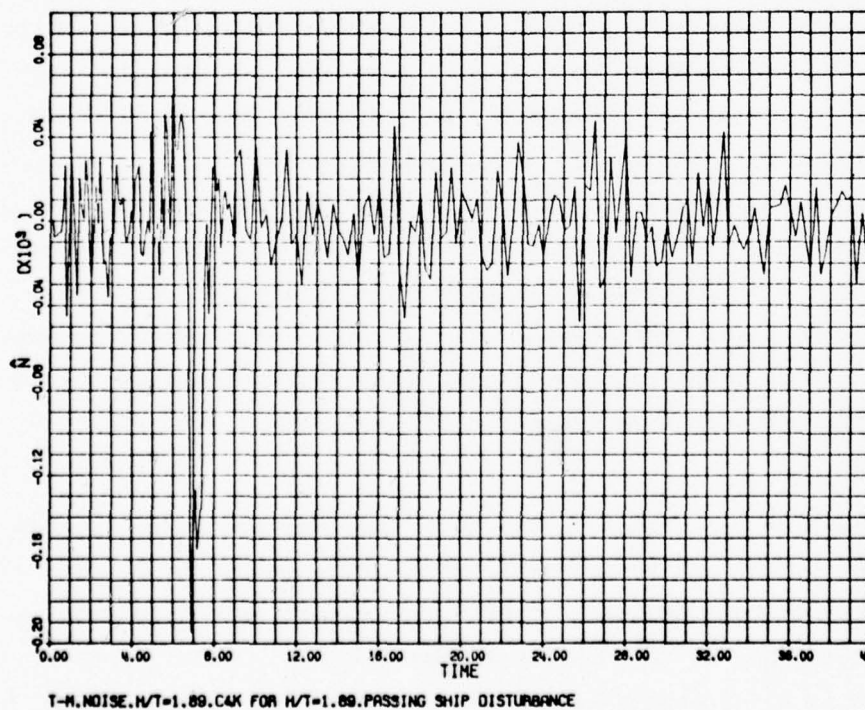
Figure 10.   Yaw Moment Estimate for Passing Ship: Optimal Control

The particular lateral offset response shown in Fig. 8 is strongly affected by the sequence of randomly generated measurement noise included in our simulation. SHIPSIM/OPTSIM[11] uses the IBM Scientific Subrouting Package random number generator subroutine RANDU to generate the sequence of random numbers which establish the noise level for each measurement at each integration step in accordance with the user-specified standard deviation σ'. To allow a valid comparison among competing control systems SHIPSIM/OPTSIM always begins with the same initial random number seed. Thus, all runs utilize the same sequence of randomly generated numbers unless the program is specifically modified to change the initial seed. When the disturbance magnitude is fairly small as used here, the response due to the disturbance is roughly comparable to the response due to the measurement noise and the maximum system response is noticeably affected by the particular sequence of measurement noise used in the simulation. The response shown in Fig. 8 is such that the ship is already moving to port ($\eta < 0$) due to measurement noise when the disturbnace due to the passing ship is first felt ($t'=5$). This causes the maximum lateral offset of the ship, which is also to port, to be increased. To clarify this, Fig. 11 shows the lateral offset response of the *Tokyo Maru* to the same passing ship disturbance when there is no noise in the measurements received by the filter; i.e., $\sigma'=0$. The maximum lateral offset is about 1.5 m. in lieu of 1.7 m. as shown in Fig. 8. It is also possible for the measurement noise to reduce the maximum lateral offset. This is illustrated by the lateral offset response in the simulation shown in Fig. 12. This simulation was conducted with a modified initial random number seed. For this sequence of measurement noise, the ship happens to be moving to starboard ($\eta > 0$) due to the measurement noise when the disturbance due to the passing ship is first felt. This causes the maximum lateral offset to port due to the passing ship to be reduced to only about 1.2 m. compared to the 1.5 m. shown in Fig. 11 with no measurement noise and the 1.7 m. shown in Fig. 8.

Simulation results can also show the degredation in controlled system response which would occur if the controller were designed to be optimal at some water depth other than the water depth in which the ship is operating. We simulated the response of the *Tokyo Maru* operating at a water depth-to-draft ratio H/T=1.89 while being controlled by a controller which was designed to
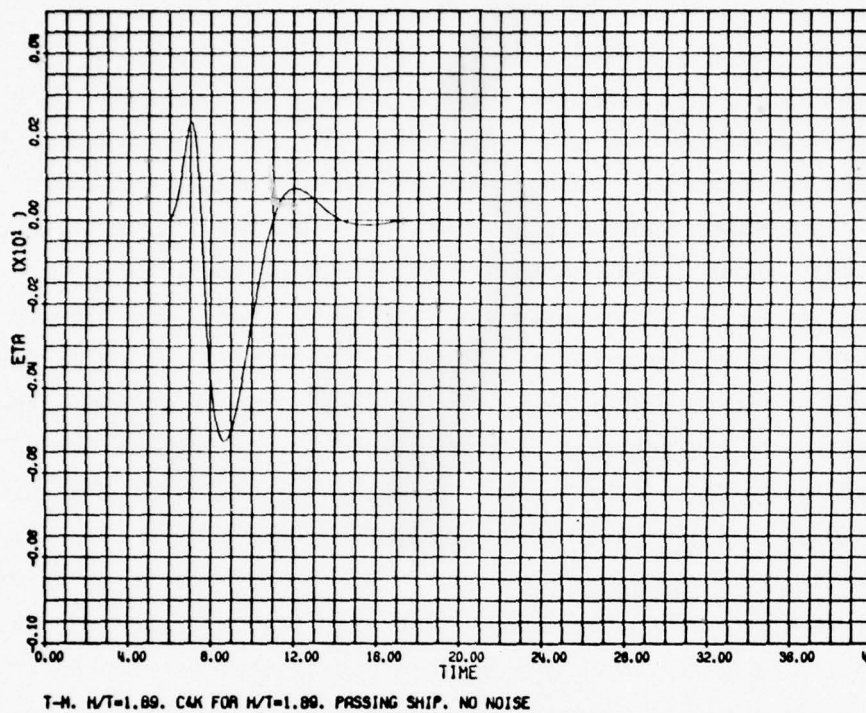
T-H. H/T=1.89. C4K FOR H/T=1.89. PASSING SHIP. NO NOISE

Figure 11. Lateral Offset Response to Passing Ship: Optimal Control; No Noise

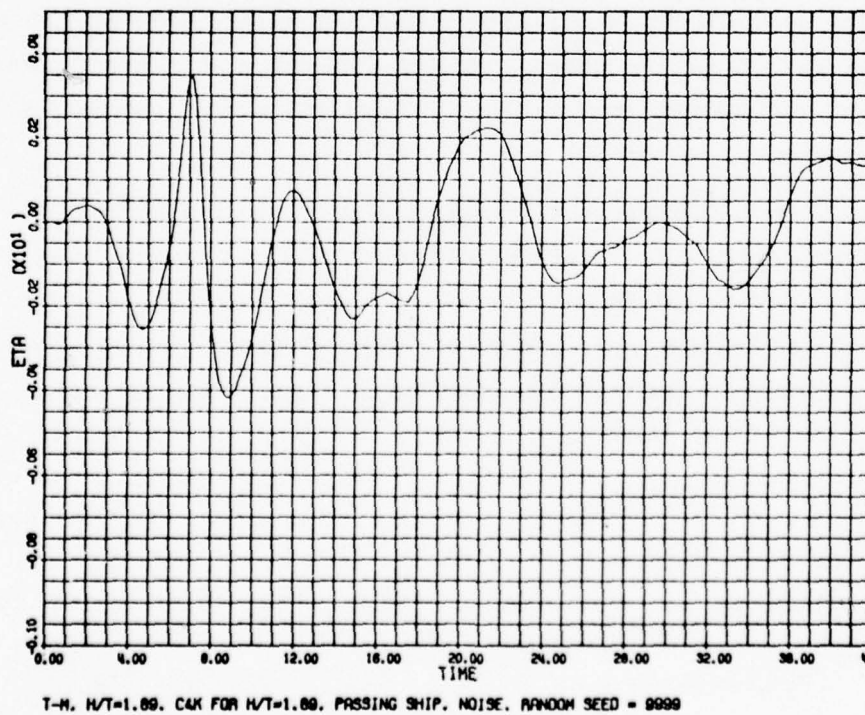T-H. H/T=1.89. C4K FOR H/T=1.89. PASSING SHIP. NOISE. RANDOM SEED = 9999

Figure 12. Lateral Offset Response to Passing Ship: Optimal Control; Modified Seed

to be optimal in deep water H/T=∞. Figure 13 shows the lateral offset
response to a B/2 initial lateral offset error. This response can be
compared directly with the response shown in Fig. 6 for the *Tokyo Maru* when
the optimal control and filter gains are used. The initial return to the
prescribed path is noticeably faster with the non-optimal, deep water
controller. The maximum overshoot however, is, about 15.4 m. in lieu of the
overshoot of only about 3.2 m. shown in Fig. 6 and it takes the ship about
4 ship lengths longer to settle onto the prescribed path. The loss in
performance with the use of non-optimal control and filter gains at H/T=1.89
is evident from a comparison of these two figures. Figure 14 shows the lateral
offset response to a passing ship as represented by the yaw moment and sway
force disturbance shown in Fig. 4 when the *Tokyo Maru* is again controlled by
a controller which was designed to be optimal at H/T=∞. This response can be
compared directly with the response shown in Fig. 8 for the *Tokyo Maru* when
controlled by the optimal controller for the existing H/T=1.89 water depth.
In this situation, the maximum response does not degrade as much as in the
initial offset simulation. The maximum lateral offset is about 1.9 m. with
the non-optimal H/T=∞ design compared to about 1.7 m. with the optimal H/T=1.89
design controller. This result could be expected based on the RMS response
results for the *Tokyo Maru* controlled by these two controllers at H/T=1.89 as
shown in Table 16. There the design for H/T=∞ showed a 14 percent increase
in RMS cost but a 16 percent *decrease* in RMS lateral offset compared to the
controller designed to be optimal at H/T=1.89.

In general, we feel that these simulation results confirm that the
optimal stochastic path controllers developed here would provide very
effective ship path control in restricted waters. The effectiveness of these
controllers will be further compared to the control which could be expected
from a human helmsman in Section 5.5 below.
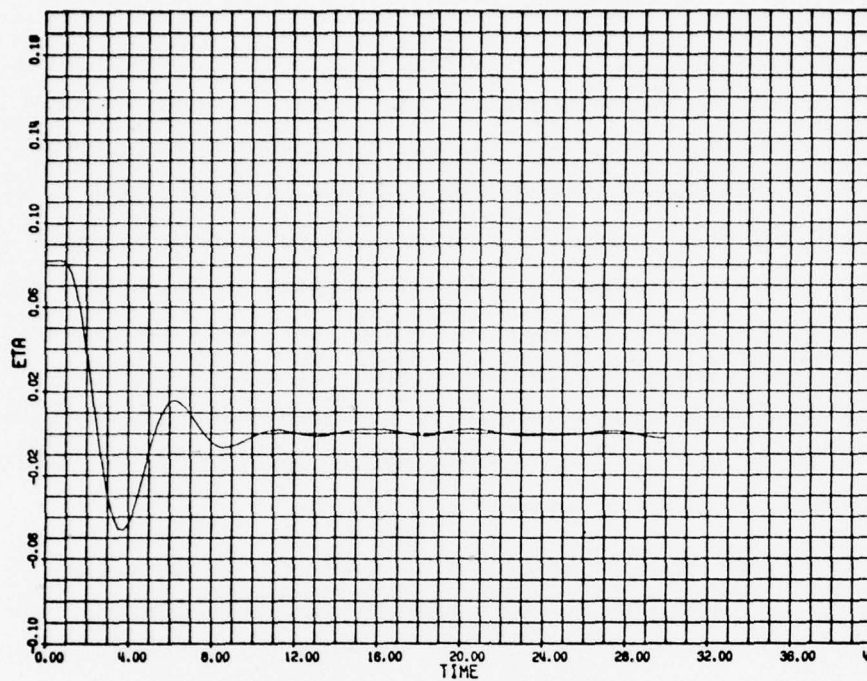
T-M.NOISE.H/T=1.89.C&K FOR H/T=INFINITY.INITIAL OFFSET 0.5=BEAM

Figure 13.   Lateral Offset Response to B/2 Initial Offset: H/T=∞ Optimal Design

T-M. NOISE. H/T=1.89. C & K FOR H/T=DEEP. PASSING SHIP

Figure 14.   Lateral Offset Response to Passing Ship: H/T=∞ Optimal Design

5.4 Verification of Disturbance Modeling

In this section, we look a little more closely at the effectiveness of the Kalman-Bucy filter to estimate the state of the ship. In particular, the effectiveness of the filter to estimate the yaw moment and sway force acting on the ship due to a passing ship is studied in more detail as a means of verifying the validity of using first-order shaping filters to model the yaw moment and sway force disturbances. We also compare the effectiveness of the optimal controller design presented in Section 3 with that of an optimal controller designed without the use of shaping filters; i.e., the yaw moment and sway force disturbances are assumed to be white noise instead of exponential correlated disturbances. We feel these results clearly show the validity of our disturbance modeling approach.

Figure 15 shows a more detailed presentation of the yaw moment distur-bance estimates $\hat{N}'$ produced by the optimal Kalman-Bucy filter in the simulation runs shown in Fig. 8, Fig. 11, and Fig. 12. Also shown in Fig. 15 for comparison is the yaw moment disturbance N' actually used in these simulations as shown in Fig. 4. The yaw moment disturbance estimate for the simulation run without measurement noise; i.e., $\sigma'=0$, represents the expected average of estimates over a large number of runs. This estimate was obtained in the simulation run shown in Fig. 11. Comparing this estimate with the actual yaw moment disturbance shows the filter to be generally very effective in estimating the yaw moment disturbance. This is remarkably fast when one considers that the filter can only estimate N' after the ship begins to respond to the disturbance and this is reflected in the measurements ψ', r', and η'. The estimate is low in peak value by about 20% for the initial positive peak and by about 13% for the maximum disturbance when the ships are beam-to-beam at $t'=7$. The filter is less effective at the final positive peak where the estimate is low by about a factor of 4. The yaw moment disturbance estimates for the simulation run using the standard measurement noise initial random number seed as shown in Fig. 8 and for the simulation run using the modified seed as shown in Fig. 12 are also shown in Fig. 15 to illustrate the effect of specific sequences of measurement noise on the estimate $\hat{N}'$ produced by the Kalman-Bucy filter.
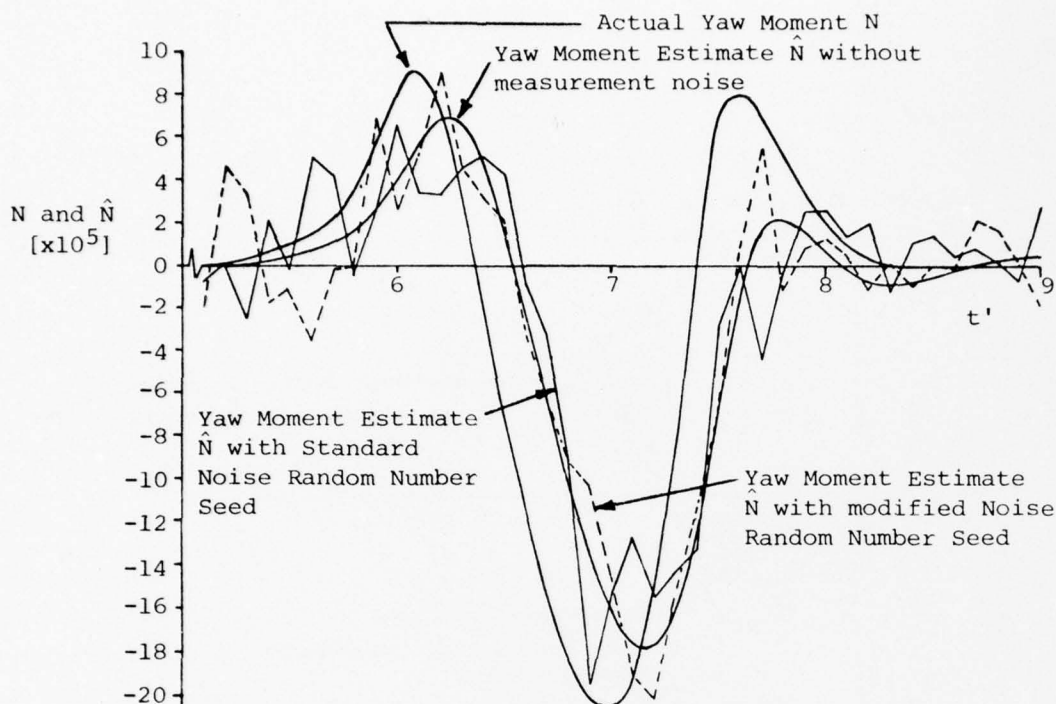
Figure 15.   Yaw Moment Disturbance Estimates for Passing Ship

Figure 16 shows the sway force disturbance estimates $\hat{Y}'$ produced by the optimal Kalman-Bucy filter in the simulation runs shown in Fig. 8, Fig. 11, and Fig. 12. The actual sway force disturbance Y' used in these simulations as shown in Fig. 4 is also shown for comparison. Again the sway force disturbance estimate for the simulation run without measurement noise represents the expected average of estimates over a large number of runs. In this situation, the filter is much less effective in estimating the sway force disturbance than it is in estimating the yaw moment disturbance. The filter is about 0.2 ship lengths behind and about a factor of 3 low in estimating the peak sway force disturbance which occurs when the ships are beam-to-beam. Since the optimal stochastic controller provides excellent response in general, this inability to estimate Y' as accurately as N' does not seem to be a practical problem.

The lack of ability of the filter to effectively estimate Y' is at first not apparent from a look at the observability of each mode of the system with each measurement as shown in Table 9. This is because each row in Table 9 reflects the relative observability of each mode with each measurement. If this Table included measurements of all seven states, the elements of each
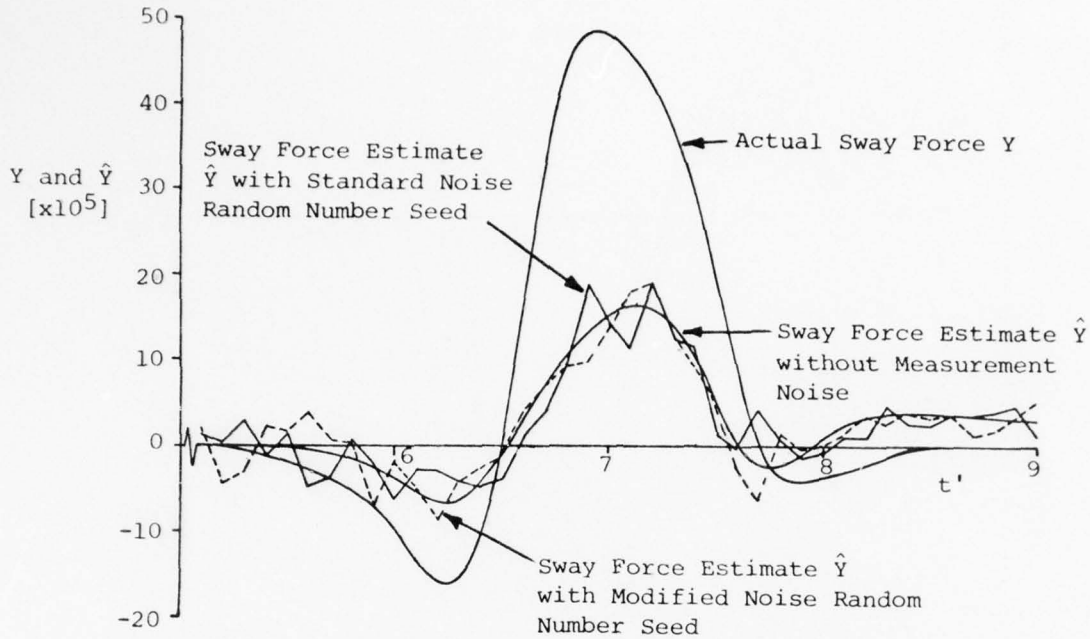
Figure 16.   Sway Force Disturbance Estimates for Passing Ship

row would be seen to be orthonormalized; i.e. $\sum_{j=0}^{n} \cos^2 \beta_{ij} = 1$, when the
measurements are just the states. These data do not reflect the *absolute*
observability of one mode compared to another. Comparisons made within each
row of Table 9 are therefore valid but numerical comparisons within each
column of Table 9 are not valid. The primary reason for the poor estimate
of Y' is due to speed at which the disturbance occurs compared to the
time constants of the controlled ship. The Y' disturbance occurs about
twice as fast as the N' disturbance and as a result is too fast to have
much of an effect on the ship. This Y' disturbance therefore has a low
level of absolute observability. A test run using a Y' disturbance which
is identical to the N' disturbance shown in Fig. 4 resulted in a good
estimate $\hat{Y}'$ and confirms this conclusion. For the same physical reasons
that Y' in Fig. 4 does not affect r', ψ', and η' significantly resulting
in a low level of absolute observability, a weak estimate $\hat{Y}'$ does not
seriously affect the overall controller performance.

The effectiveness and validity of modeling yaw moment and sway force
disturbances as first-order filters in the optimal stochastic controller
design can be further illustrated by comparing this controller with an optimal

controller design developed for the *Tokyo Maru* at H/T=1.89 without the use
of the shaping filters. In this case, the yaw moment and sway force distur-
bances were considered to be white noise with power spectral densities given
by eq. (56) and eq. (57). The resulting optimal design produces feedback
gains on ψ', r', β', η', and δ' which are identical to those presented in
Section 3 for the design which utilizes the shaping filter modeling of the
disturbances. The closed-loop eigenvalues are therefore identical to the
first five eigenvalues shown for this design in Table 12. The dimension of
the Kalman-Bucy filter is reduced to 5; i.e., $\hat{x}$ includes just the system
states and not the yaw moment and sway force disturbances. Table 22 shows
the RMS response of the optimal controller designed for the *Tokyo Maru* at
H/T=1.89 without shaping filters with that of the optimal controller designed
using shaping filters. This latter data is a repeat of that given in Tables
11 and 16. The RMS cost increases 3.5 times when the shaping filters are not
used in the design; the RMS lateral offset from the prescribed path increases
from 3.55 m. when shaping filters are used to 8.61 m. The control system
developed without the use of the shaping filters is much less effective
based on the RMS response to the design disturbances.

	without shaping filters	with shaping filters
$\tilde{\psi}'$	.02108 (1.21°)	.00755 (.43°)
$\tilde{r}'$	.03342	.00876
$\tilde{\beta}'$	.00898	.00501
$\tilde{\eta}'$	.02968 (8.61m)	.01223 (3.55m)
$\tilde{\delta}'$	.07651 (4.4°)	.04521 (2.6°)
$\tilde{\delta}_c'$	.09044	.05180
$\tilde{J}$	.01966	.00566

Table 22. RMS Response with Optimal Controllers Designed
with and without Shaping Filters

A comparison of the effectiveness of the optimal controllers designed
with and without the use of shaping filters to model the yaw moment and sway
force disturbances is perhaps clearest when simulation results are studied.

Figure 17 shows the lateral offset response of the *Tokyo Maru* at H/T=1.89
to the passing ship disturbance shown in Fig. 4 when the ship is controlled
by the optimal controller developed without the use of shaping filters to
model the disturbances.   This response can be compared directly with the
response shown in Fig. 8 for the *Tokyo Maru* controlled by the optimal controller
developed with the use of shaping filters.   The maximum lateral offset in
Fig. 17 is 4.9 m. compared to 1.7 m. shown in Fig. 8.   Thus the use of
shaping filters to model the disturbances results in an optimal stochastic
controller design which is almost three times as effective in limiting the
lateral offset from the prescribed path when a ship passes.   Figure 18 shows
the rudder usage in the simulation shown in Fig. 17.   The maximum rudder
angle is about 5.3° compared to a maximum of about 6.9° shown in Fig. 9.

T-M.NOISE.PASSING SHIP.H/T=1.89.OPTIMAL.NO FILTER.INT.STP=0.001

Figure 17.   Lateral Offset Response to Passing Ship: Optimal Design
without Shaping Filters

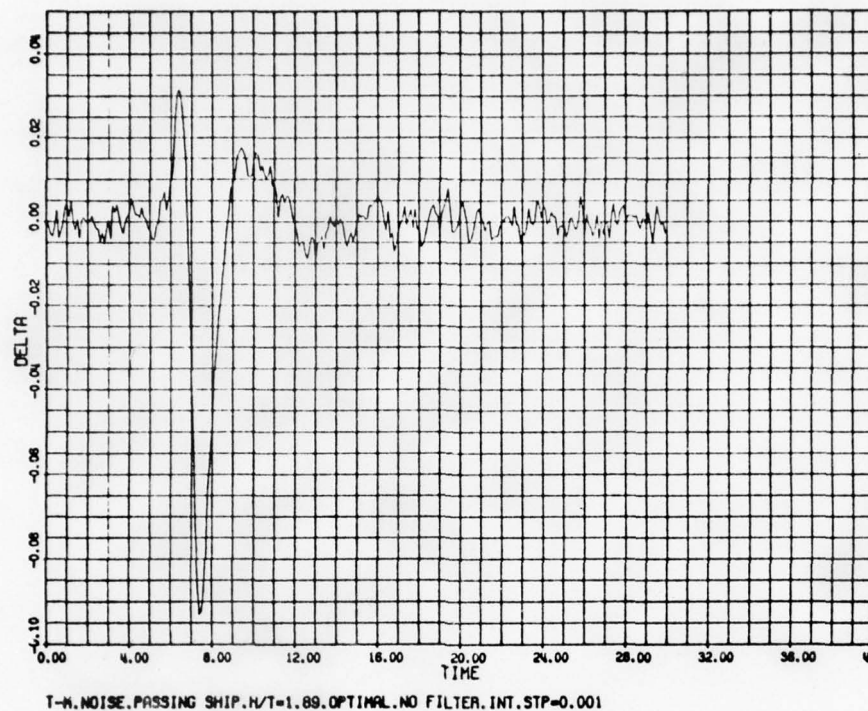T-H.NOISE.PASSING SHIP.H/T=1.89.OPTIMAL.NO FILTER.INT.STP=0.001

Figure 18.   Rudder Angle Response to Passing Ship: Optimal Design
without Shaping Filters

5.5 Comparison with Human Helmsman Control

The final simulation results to be presented are a comparison between the
control provided by the optimal stochastic controllers developed here and the
control which might be expected by a human helmsman. To be judged effective,
the stochastic controllers should probably be at least as good as a human.
If the two were about equal based on typical performance, the automated
control might still be justified and desirable since it is the "human error"
and occasionally bad, non-typical human performance which usually gets a
ship into trouble. An automated system could provide a more consistent,
repeatable performance which would be less affected by fatigue, stress,
distractions, etc.

In order to perform a digital computer simulation representing human
helmsman control, a human model must be available. Suitable human models for
ship control research are very limited. Human models for the ship *heading*
control problem have been presented by Hooft[25] and Stuurman.[26] These can be

shown to be essentially equivalent. Stuurman presents data for a single
ship. Hooft presents specific data for helmsmen control for a wide range of
course-stable ships. For our work, we adapted Hooft's model to apply to path
control and have extrapolated his data to apply to the *Tokyo Maru* in deep
water where the ship is course stable. It would be expected that the helmsman
would be less effective in controlling the *Tokyo Maru* at H/T=1.89 where it is
course unstable but the human model data necessary to allow simulation at
this water depth is not available.

Hooft's model for human heading control was derived from the response of
helmsmen who were instructed to steer a ship in a land-based simulator along
a prescribed sinusoidal path. In the modeling, he first assumed that the
rudder angle δ would be positioned proportional to the course error $\Delta\psi$
and the yaw rate error Δr; i.e.,

$$\delta = k_1\Delta\psi + k_2\Delta r \quad . \tag{97}$$

He then assumed the helmsman would compare the existing rudder angle δ with
that required rudder angle $\delta^*=k_3\psi$ needed to steer along the prescribed
sinusoidal course. This gives an error between the existing and required
rudder angles,

$$\Delta\delta^* = \delta^*-\delta \quad , \tag{98}$$

or,

$$k_3\Delta\psi = k_3\psi-\delta \quad , \tag{99}$$

which gives,

$$\Delta\psi = \psi-\delta/k_3 \quad . \tag{100}$$

Combining eq. (97) and (100) yields Hooft's helmsman heading control transfer
function,

$$G(s) = \frac{\delta(s)}{\Delta\psi(s)} = \frac{k_1 k_3}{k_1+k_3} \; \frac{\frac{k_2}{k_1}s+1}{\frac{k_2}{k_1+k_3}s+1} = a\;\frac{T_L s+1}{T_N s+1} \quad . \tag{101}$$

Hooft conducted the simulator experiments with helmsmen to establish the
parameters a, T_L, and T_N. Since the helmsmen respond differently

when controlling different types of ships, Hooft obtained his data as functions of the K and T in Nomoto's maneuvering equation[27]; i.e.,

$$T\dot{r} + r = K\delta \quad .$$ (102)

The data a, T_L, and T_N therefore apply to a wide range of ship dynamics but were unfortunately limited to course-stable ships.

Hooft's model does not apply directly to ship *path* control but provides the best available helmsman model. We therefore adapted the model to path control by assuming that the transfer function eq. (101) applied not just to a heading error $\Delta\psi$ but to an error function which includes a weighted sum of a heading error, a yaw rate error, and a lateral deviation error. We thus used,

$$G(s) = \frac{\delta(s)}{e(s)} = a\frac{T_L s+1}{T_N s+1} \quad ,$$ (103)

where the error function was given by,

$$e = B_1(\psi-\psi_o)+B_2(r-r_o)+B_3(\eta-\eta_o) = B_1\psi+B_2 r+B_3\eta \quad ,$$ (104)

since $\psi_o=r_o=\eta_o=0$ on the prescribed path. To implement the transfer function in the simulation, eq. (103) was first written,

$$G(s) = a\frac{T_L}{T_N}\frac{s+1/T_L}{s+1/T_N} = A\frac{s+1/T_L}{s+1/T_N} \quad ,$$ (105)

which can then be implemented by an additional state-variable equation representing an internal helmsman state,

$$\dot{y}' = -\frac{1}{T_N'}y' + A(B_1\psi'+B_2 r'+B_3\eta') \quad ,$$ (106)

and a rudder command equation,

$$\delta_c' = \left(\frac{T_N'-T_L'}{T_N' T_L'}\right)y' + A(B_1\psi'+B_2 r'+B_3\eta') \quad .$$ (107)

These equations were used in a simulation to approximate helmsman path control of the *Tokyo Maru* at $H/T=\infty$. In nondimensional form, Hooft's data yields A=13.20, $T_N'=0.6630$, and $T_L'=0.5835$ for the *Tokyo Maru* characteristics at $H/T=\infty$.

Since the helmsman model was only available for a course-stable condition, the helmsman results cannot be compared directly with the optimal stochastic controller simulations performed at H/T=1.89 and presented above. The optimal stochastic controller designed for deep water was therefore simulated with the passing ship disturbance shown in Fig. 4 to provide a basis for comparison with helmsman control. Lateral offset response is shown in Fig. 19. Since the *Tokyo Maru* is course stable at H/T=∞, the optimally controlled ship is also more course stable than at H/T=1.89. The maximum lateral offset is only 0.75 m. compared to the 1.7 m. shown in Fig. 8 for H/T=1.89. The rudder angle response is shown in Fig. 20. The maximum rudder angle is about 6.4°. The degredation of controller performance with changing water depth can be further seen by comparing the results shown in Fig. 19 and Fig. 14. The performance of the optimal controller operating at its design depth H/T=∞ degrades in maximum lateral offset response from the 0.75 m. shown in Fig. 19 to the maximum response of 1.9 m. shown in Fig. 14 as the ship is brought into the shallower, H/T=1.89 water.
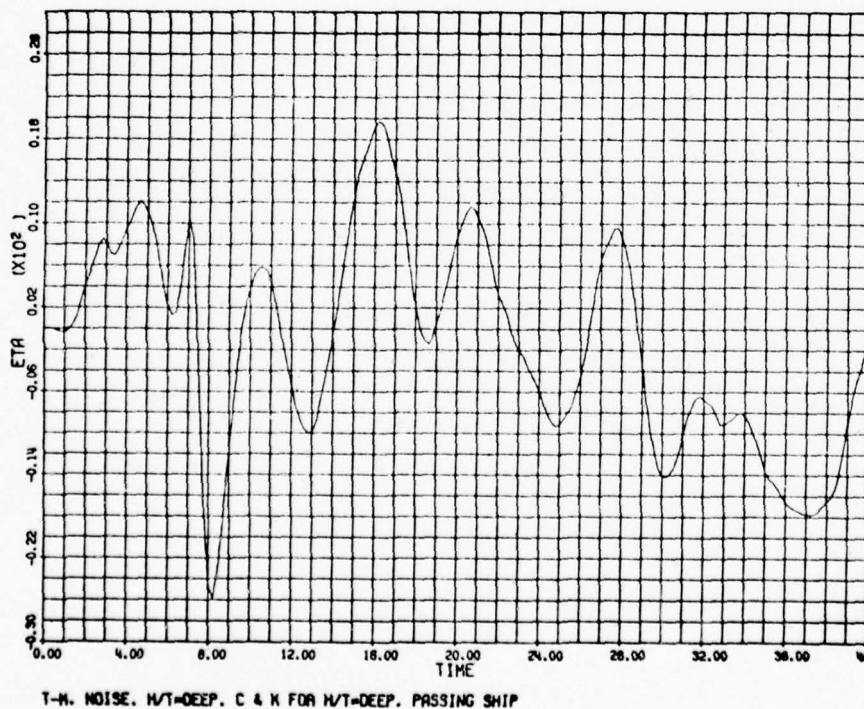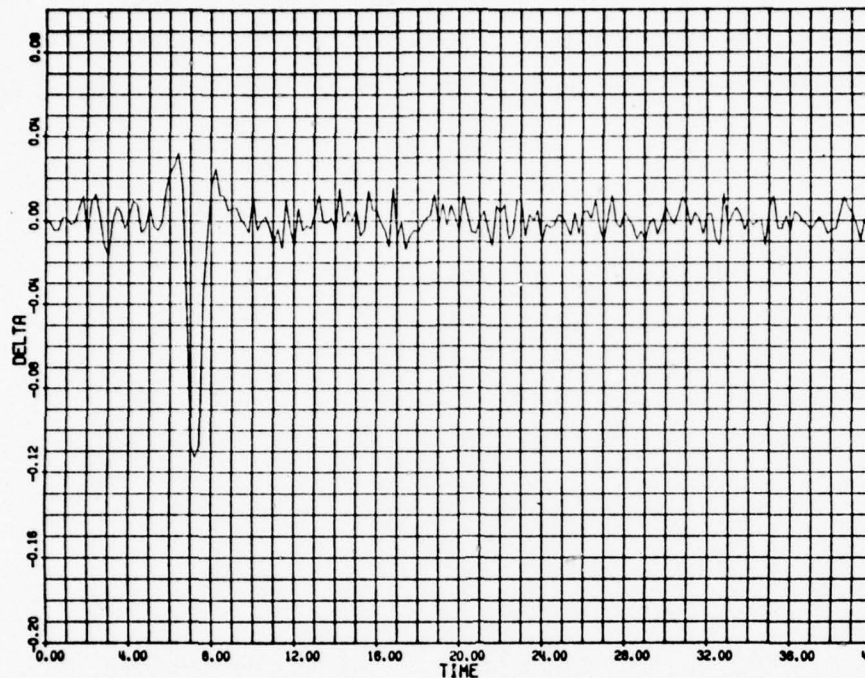

T-M. NOISE. H/T=DEEP. C & K FOR H/T=DEEP. PASSING SHIP

Figure 19.   Lateral Offset Response to Passing Ship: Optimal Control at H/T=∞

T-M. NOISE. H/T=DEEP. C & K FOR H/T=DEEP. PASSING SHIP

Figure 20. Rudder Angle Response to Passing Ship: Optimal Control at H/T=∞

The response of the *Tokyo Maru* to the passing ship disturbance shown in Fig. 4 while operating at H/T=∞ under control of the helmsman defined by eq. (106) and (107) is shown in Fig. 21 and Fig. 22. For these simulations we have used $B_1=0.8$, $B_2=0.1$, and $B_3=0.1$. These quantities include both weighting considerations and scaling differences among ψ', r', and η' errors. For these simulations, the helmsmen was given the *same* noisy measurements used by the stochastic controller. This is very conservative since human reaction to a measurement display will introduce additional error. Further, the helmsman will not read each measurement at each decision point. This will be particular evident in the η measurement if there is no automated output of the lateral offset from the prescribed path and the helmsman or an assistant must establish η manually from a radar screen. The lateral offset response in Fig. 21 can be compared directly with the response with the optimal stochastic controller as shown in Fig. 19. The maximum lateral offset response is 1.5 m. compared to the 0.75 m. shown in Fig. 19. The maximum rudder angle response in Fig. 22 is about 10.3° which can be compared directly

with the 6.4° maximum rudder angle shown in Fig. 20.   In general, the optimal
stochastic controller provides a level of control which is superior to that
provided by a helmsman given by Hooft's model as implemented in eq. (106) and
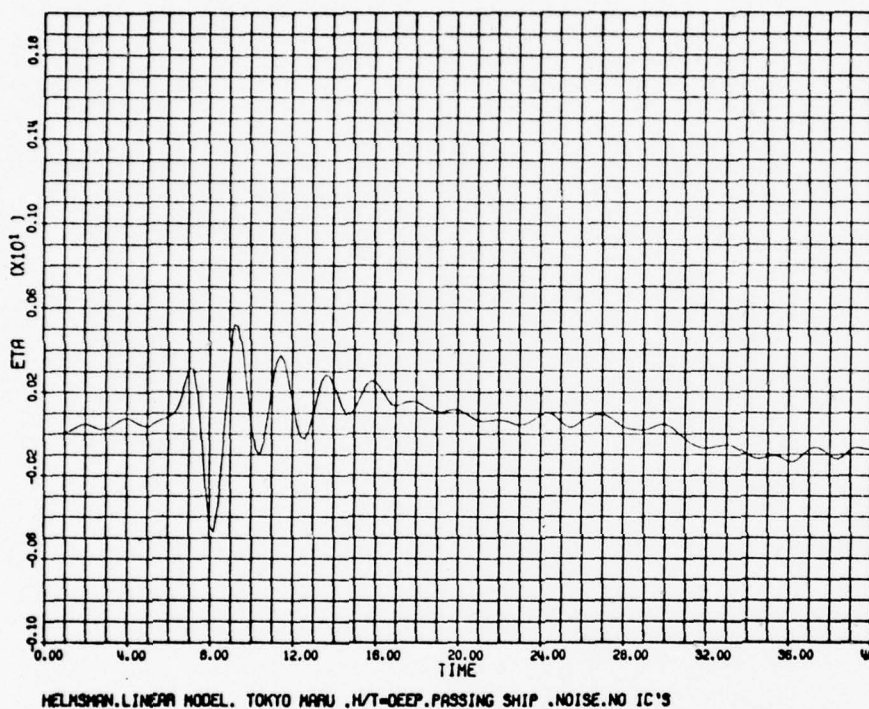eq. (107).

Figure 21.   Lateral Offset Response to Passing Ship: Helmsman Control at $H/T=\infty$
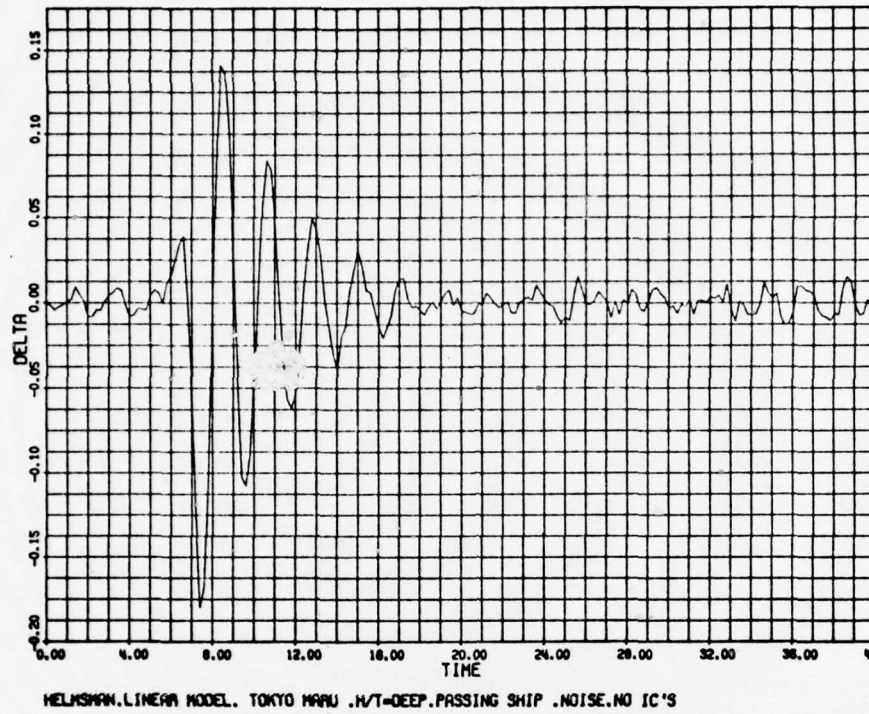
HELMSMAN.LINEAR MODEL. TOKYO MARU .H/T=DEEP.PASSING SHIP .NOISE.NO IC'S

Figure 22.   Rudder Angle Response to Passing Ship: Helmsman Control at H/T=∞

6. Performance of Partially-Adapted Controllers

This final section presents the results of an evaluation of the need to adapt path control systems for water depth dependent changes in the various terms in the equations of motion. In general, the optimal stochastic path controllers studied here provide very effective control. In Section 2, we showed how the ten coefficients f_{ij} and γ_{ij} in the linear equations of motion for a ship moving along a prescribed straight-line path vary with both water depth and vessel speed. In Section 4, we studied the effect of water depth and vessel speed on the design and performance of the optimal stochastic path controllers. For ships such as the *Tokyo Maru* which are course unstable at some water depth-to-draft ratios H/T, we concluded that if a design is to be optimal at a single water depth (constant C and K gain matrices) it should be designed to be optimal at the depth-to-draft ratio at which the ship is least course stable. For these course-unstable ships, however, we noted the need for an adaptive path control system which could automatically adjust the C and K gain matrices to be optimal at any operating H/T. In these systems, the coefficients f_{ij} and γ_{ij} could be identified on-line along with the estimation of $\hat{\underline{x}}$. The C and K matrices could then be updated to remain optimal and reflect the changing ship characteristics with changing H/T.

The need to simultaneously identify all ten coefficients in eq. (28); i.e., f_{22}, f_{23}, f_{25}, γ_{21}, γ_{22}, f_{32}, f_{33}, f_{35}, γ_{31}, γ_{32}, could greatly complicate the design of an adaptive path controller. We therefore performed a sensitivity study to see how important it would be to adapt for changes in each of the individual coefficients. If a specific coefficient were not to be identified on-line, the controller design would most likely be based on the value of that coefficient at the ship's least course-stable water depth-to-draft ratio. The study was therefore conducted by first using the OPTSYS program to design optimal controller gains C and K for the *Tokyo Maru* using the F_e matrix in eq. (58) which has all coefficients f_{ij} correct for H/T=∞ except one. The value of this remaining coefficient was set at its value at H/T=1.89, the ship's least course-stable condition. This simulates the gain matrices which a partially-adapted path controller would produce if it were to identify all coefficients except the one while the ship is operating at H/T=∞. The

-66-

resulting gain matrices were then used again in the OPTSYS program with the F_e matrix which was fully correct for $H/T=\infty$ to establish the resulting RMS response and closed-loop eigensystem. This is the response of the ship at $H/T=\infty$ while under control of the partially-adapted controller which identifies all coefficients except the one. This process was repeated for each of the coefficients in succession in order to establish a quantitative sensitivity measurement which indicates how important it would be to adapt for the changes in each of the individual coefficients. An adaptive controller which would only need to identify and adapt for changes in two or three instead of ten coefficients might be greatly simplified and therefore be more feasible.

The RMS response results for the *Tokyo Maru* at $H/T=\infty$ with the partially-adapted controllers are shown in Table 23. Also shown for comparison are the RMS response when the ship is controlled by the optimal controller for the existing $H/T=\infty$, which represents the fully-adapted controller, and the RMS response with the optimal controller designed for the ship's least course-stable water depth of $H/T=1.89$, which represents the non-adapted controller. The results are arranged in the order of increasing RMS cost $\tilde{J}$; i.e., the order of increasing importance for adaptation. Based on the RMS cost, seven of the coefficients (γ_{31}, f_{35}, γ_{22}, f_{33}, f_{22}, γ_{32}, and f_{32}) have very little effect on the response if the controller does not adapt for their changes individually. Two of the coefficients γ_{21} and f_{25} have a somewhat larger effect on the RMS response. The final coefficient f_{23}, the coefficient of β' in the $\dot{r}'$ state equation (13), has by far the greatest importance based on this measure. Notice that the three most important coefficients are all in the $\dot{r}'$ state equation. Notice also that these coefficients do not necessarily experience the largest numerical variations with H/T shown in Table 4. An adaptive control system could probably provide most of the potential improvement in performance to be gained with adaptation if only f_{23}, f_{25}, and γ_{21} were identified on-line. To verify this conclusion, we repeated the partially-adapted controller design and evaluation process for the case where the design did not adapt for all seven of the coefficients γ_{31}, f_{35}, γ_{22}, f_{33}, f_{22}, γ_{32}, and f_{32} simultaneously. This represents the situation where the controller would adapt only for changes in the coefficients f_{23}, f_{25}, and γ_{21} with water depth. The RMS cost $\tilde{J}$ in this case was 0.00683. The cumulative effect of not adapting for the changes in seven of the coefficients

	fully-adapted optimal at $H/T=\infty$	all adapted except γ_{31}	all adapted except f_{35}	all adapted except γ_{22}
$\tilde{\psi}'$	0.00965	0.00966	0.00967	0.00960
$\tilde{r}'$	0.00982	0.00982	0.00984	0.00976
$\tilde{\beta}'$	0.00834	0.00834	0.00835	0.00832
$\tilde{\eta}'$	0.01607	0.01609	0.01607	0.01610
$\tilde{\delta}'$	0.04773	0.04771	0.04774	0.04770
$\tilde{\delta}_c'$	0.05406	0.05404	0.05405	0.05405
$\tilde{J}$	0.00681	0.00681	0.00681	0.00681
	all adapted except f_{33}	all adapted except f_{22}	all adapted except γ_{32}	all adapted except f_{32}
$\tilde{\psi}'$	0.00946	0.00966	0.00955	0.01032
$\tilde{r}'$	0.00968	0.00963	0.00968	0.01047
$\tilde{\beta}'$	0.00831	0.00831	0.00830	0.00850
$\tilde{\eta}'$	0.01590	0.01616	0.01611	0.01629
$\tilde{\delta}'$	0.04783	0.04755	0.04770	0.04780
$\tilde{\delta}_c'$	0.05432	0.05410	0.05409	0.05365
$\tilde{J}$	0.00681	0.00682	0.00682	0.00683
	all adapted except γ_{21}	all adapted except f_{25}	all adapted except f_{23}	non-adapted optimal at $H/T=1.89$
$\tilde{\psi}'$	0.01029	0.00834	0.00846	0.00850
$\tilde{r}'$	0.01038	0.00855	0.00769	0.00753
$\tilde{\beta}'$	0.00841	0.00806	0.00768	0.00756
$\tilde{\eta}'$	0.01775	0.01539	0.02066	0.02238
$\tilde{\delta}'$	0.04690	0.04824	0.04556	0.04533
$\tilde{\delta}_c'$	0.05224	0.05599	0.05279	0.05249
$\tilde{J}$	0.00689	0.00693	0.00746	0.00783

Table 23. RMS Response with Partially-Adapted Controllers at $H/T=\infty$

increases the cost only about 0.3 per cent and is no worse than the effect of just the most important of these f_{32} .

The closed-loop eigenvalues for the *Tokyo Maru* at H/T=∞ with the partially-adapted controllers are shown in Table 24. Also shown for comparison are the closed-loop eigenvalues when the ship is controlled by the optimal controller for the existing H/T=∞ (the fully-adapted controller) and the closed-loop eigenvalues with the controller designed to be optimal at H/T=1.89 (the non-adapted controller). The coefficients γ_{21}, γ_{22}, γ_{31}, and γ_{32} do not affect the feedback control gain matrix C and thus partially-adapted controllers which do not adapt for these coefficients have the same closed-loop eigenvalues as the fully-adapted case. These coefficients do affect the filter gains K and therefore affect the RMS response as shown in Table 23. The partially-adapted controller closed-loop eigenvalues are presented in Table 24 for the remaining coefficients. These results are presented in the order of increasing importance for adaptation based on RMS cost $\tilde{J}$ as shown in Table 23. The dominant closed-loop eigenvalues for these partially-adapted controllers and the fully-adapted and non-adapted controllers are shown in Fig. 23. Again, coefficient f_{23} is the most important single coefficient and as a minimum an adaptive system should identify f_{23} on-line and update the control and filter gain matrices to reflect changes in f_{23} with water depth. Adaptation for changes in coefficients f_{25} and γ_{21} would also appear justified.
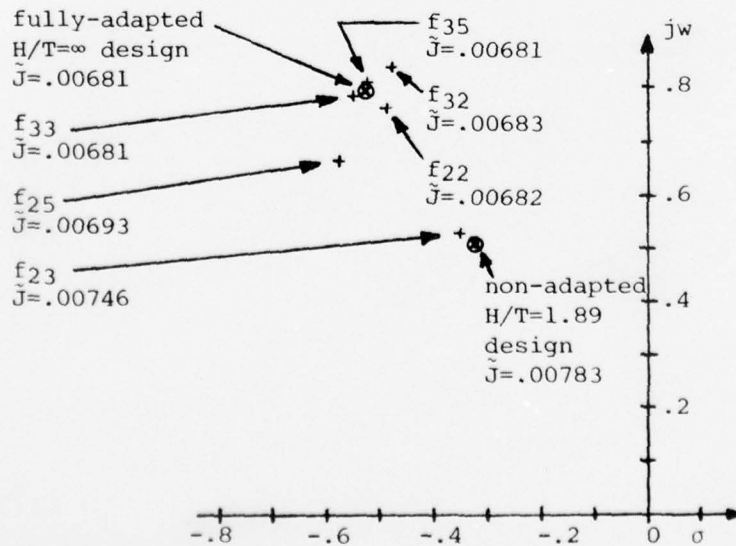

Figure 23. Dominant Closed-loop Eigenvalues with Partially-Adapted Controllers

fully-adapted optimal at $H/T=\infty$	all adapted except f_{35}	all adapted except f_{33}	all adapted except f_{22}
$-.5226 \pm .7991$ j	$-.5218 \pm .8008$ j	$-.5446 \pm .7908$ j	$-.4820 \pm .7628$ j
-0.8913	-0.8903	-0.8838	-0.9357
-2.476	-2.476	-2.470	-2.667
-7.470	-7.463	-7.468	-7.396
-1.000	-1.000	-1.000	-1.000
-1.000	-1.000	-1.000	-1.000

all adapted except f_{32}	all adapted except f_{25}	all adapted except f_{23}	non-adapted optimal at $H/T=1.89$
$-.4725 \pm .8382$ j	$-.5756 \pm .6679$ j	$-.3496 \pm .5331$ j	$-.3208 \pm .5111$ j
-0.8893	-1.102	$-2.115 \pm .7323$ j	$-2.249 \pm .9161$ j
-2.434	-2.472		
-7.499	-7.093	-7.378	-6.997
-1.000	-1.000	-1.000	-1.000
-1.000	-1.000	-1.000	-1.000

Table 24.   Closed-loop Eigenvalues with Partially-Adapted Controllers at $H/T=\infty$

7. Conclusions

The principal general conclusions of this work are summarized here for reference.

- With sufficient measurements, the optimal stochastic path controllers as developed here can provide very effective control of a surface ship in shallow water. Measurement of lateral offset is necessary. Additional measurements of heading and yaw rate are needed to provide effective control. The further addition of a drift angle measurement from a doppler sonar is not justified.

- The water depth-to-draft ratio H/T can have significant effect on the performance of optimal stochastic path controllers when they are designed for a specific water depth and then operated over the feasible range of water depths. The effect of speed changes on the performance of fixed-gain controllers is less than the effect of changes in depth-to-draft ratio.

- The effect of operating an optimal stochastic path controller at a speed which is slower than its design speed appears opposite to the effect of operating in a water depth which is shallower than its design depth-to-draft ratio. As a result, operation at a condition which is slower and shallower than the design condition provides performance closer to optimal than operation at the controller's design speed in the same, shallower depth water.

- Constant gain stochastic path controllers should be designed to be optimal at the ship's least course-stable open-loop water depth-to-draft ratio. For ships which are course-stable under all depth-to-draft ratios, this approach should provide a robust design which provides very effective control under all conditions.

- For ships which are course-unstable under some conditions, constant gain stochastic path controllers which are designed to be optimal at the ship's least stable open-loop condition should provide effective control under all conditions. Significant improvement in performance will be possible for these ships, however, with the use of an adaptive control system which can adjust the gains to remain optimal or near optimal for all operating conditions.

· Two features of the control and filter gains could be utilized to simplify the optimal stochastic controller implementation and adaptation. The control gain on lateral offset is constant independent of ship type, vessel speed, and water depth. Filter gains for the rudder angle estimate are zero independent of ship type, vessel speed, and water depth.

· Digital computer simulation confirms the very effective performance of the optimal stochastic path controllers. Simulation also confirms the validity of using first-order shaping filters to model the design passing ship yaw moment and sway force disturbances. The Kalman-Bucy filter is very effective in estimating the yaw moment disturbance but much less effective in estimating the sway force disturbance. The poor sway force estimate occurs because the sway force has a relatively small influence on the ship. Fortunately, the filter's poor estimate of the sway force disturbance does not degrade the effectiveness of the controller for exactly the same reason.

· A comparison of simulations of the *Tokyo Maru* controlled by an optimal stochastic path controller and by the helmsman heading control model presented by Hooft and adapted here for path control show the optimal stochastic path controller to provide a superior level of control. This conclusion is only as valid as the human helmsman modeling used.

· The optimal stochastic path controllers developed here are designed to estimate and control zero-mean disturbances. As a result, these designs cannot accommodate a continuous, non-zero-mean disturbance such as a lateral current. These disturbances can be accommodated by including two additional shaping filters for a constant yaw moment bias and a sway force bias in the design. We are proceeding with the development and study of these controllers. These results will be reported separately later.

· The sensitivity study conducted by the design and evaluation of partially-adapted controllers shows that an adaptive path control system could be almost as effective as the optimal (99.7 percent as

effective for the *Tokyo Maru* based on the RMS cost $\tilde{J}$) if it were
to identify and adapt for changes in only *three* of the ten coefficients
in the system equations which change with depth-to-draft ratio.
Coefficient f_{23} of β' in the $\dot{r}'$ equation is of greatest impor-
tance. Coefficient f_{25} of δ' and γ_{21} of N' in the $\dot{r}'$
equation are also of significance. Changes in the remaining seven
coefficients with depth-to-draft ratio have a negligible effect on
the controller performance. We are proceeding with a development
and study of adaptive ship path controllers. These results will be
reported separately later.

8. References

1. Fujino, M., "Studies on Manoeuvrability of Ships in Restricted Waters," <u>Selected Papers from the Journal of the Society of Naval Architects of Japan</u>, Vol. 4, 1970, pp. 157-184.

2. Fujino, M., "Maneuverability in Restricted Waters: State of the Art," The University of Michigan, Department of Naval Architecture and Marine Engineering, Report No. 184, Aug., 1976.

3. Bryson, A.E., Jr., and Ho, Y.C., <u>Applied Optimal Control</u>, Blaisdell, Waltham, Mass., 1969.

4. Bryson, A.E., Jr., "Control Theory for Random Systems," <u>Proceedings</u> of the Thirteenth International Congress of Theoretical and Applied Mechanics, Moscow, Aug., 1972.

5. Gelb, A. (ed), <u>Applied Optimal Estimation</u>, The MIT Press, Cambridge, Mass., 1974.

6. Timman, R., "Control Theory with Applications to Naval Hydrodynamics - The First David W. Taylor Lectures April, 1972", David Taylor NSRDC Report 4397, December, 1975.

7. Zuidweg, J.K., "Automatic Guidance of Ships as a Control Problem," Doctoral Dissertation, Delft Technical University, 1970.

8. Zuidweg, J.K., "Automatic Track Keeping as a Control Problem," Third Ship Control Systems Syposium, Paper II B-1, Bath, U.K., September, 1972.

9. Millers, H.F., "Modern Control Theory Applied to Ship Steering, " <u>Proceedings</u> of the IFAC/IFIP Symposium on Ship Operation Automation, Oslo, Norway, July, 1973.

10. Bryson, A.E., Jr., and Hall, W.E., Jr., "Optimal Control and Filter Synthesis by Eigenvector Decomposition," Stanford University Report SUDAAR No. 436, November, 1971.

11. Parsons, M.G., and Greenblatt, J.E., "SHIPSIM/OPTSIM Simulation Program for Stationary, Linear Optimal Stochastic Control Systems," ONR Report ONR-CR215-249-1, 23 June 1977.

12. Ogilvie, T.F., "Recent Progress Toward the Understanding and Prediction of Ship Motions," <u>Proceedings</u> of the 5th Symposium on Naval Hydrodynamics, Bergen, Norway, September 10-12, 1964, pp. 3-80.

13. Frank, T. et al, "Transient-maneuver Testing and the Equations of Maneuvering," <u>Proceedings</u> of the 11th Symposium on Naval Hydrodynamics, London, UK, March 28-April 2, 1976, pp. I.3-I.22.

14. Fujino, M., "The Effect of Frequency Dependence of the Stability Derivatives on Maneuvering Motions," *International Shipbuilding Progress*, Vol. 22, No. 256, December, 1975, pp. 416-432.

15. Loeser, D.J., "Determination of Maneuvering Properties in Shallow Water by Impulse Response Techniques," SNAME North California Section Paper presented April 14, 1977.

16. Chen, C.T., *Introduction to Linear System Theory*, Holt; Rinehart and Winston, Inc., New York, 1970, pp. 39-49 and pp. 189-197.

17. Parsons, M.G., "Optimal Control of Linear Systems," University of Michigan, Department of Naval Architecture and Marine Engineering, unpublished notes, Sept., 1976.

18. Severance, R.W., Jr., "Optimum Filtering and Smoothing of Buoy Wave Data," *Journal of Hydronautics*, Vol. 9, No. 2, April, 1975, pp. 69-74.

19. MacFarlane, A.G.J., "An Eigenvector Solution of the Optimal Linear Regulator Problem," *Journal of Electronics and Control*, Vol. 14, No. 6, June 1963, pp. 643-654.

20. Potter, J.E., "Matrix Quadratic Solutions," SIAM *Journal of Applied Mathematics*, Vol. 14, No. 3, May, 1966, pp. 496-501.

21. Newton, R.N., "Interaction Effects Between Ships Close Aboard in Deep Water," DTMB Report 1461, 1960.

22. Yung, T.-W., "Hydrodynamic Interactions Between Ships in Shallow Water," Ph.D. Dissertation, University of Michigan, Department of Naval Architecture and Marine Engineering, January, 1977.

23. Abkowitz, M.A., Ashe, G.M., and Fortson, R.M., "Interaction Effects of Ships Operating in Proximity in Deep and Shallow Water," *Proceedings* of the 11th Symposium on Naval Hydrodynamics, London, UK, March 28-April 2, 1976, pp. VII.37-VII.57.

24. "Doppler Sonar Docking System, MF-1005, MF100 DP," Furuno Electric Co., Ltd., Catalog No. M1101, Nishinomiya City, Japan.

25. Hooft, J.P., "The Maneuverability of Ships on a Straight Course," *International Shipbuilding Progress*, Vol. 15, No. 162, Febr. 1968, pp. 44-68.

26. Stuurman, A.M., "Human Transfer Function in Ship Steering, The Effect of Feel of the Wheel," *Proceedings* of the 4th Ship Control Systems Symposium, The Hague, The Netherlands, October 27-31, 1975, pp. 6-112 to 6-130.

27. Nomoto, K., "Analysis of Kempf's Standard Maneuver Test and Proposed Steering Quality Indices," *First Symposium on Ship Maneuverability*, DTMB Report 1461, 1960.

DISTRIBUTION LIST

Office of Naval Research
Department of the Navy
Arlington, VA. 22217
Attn: Mr. D. S. Siegel, Code 211   4
       Dr. S. Brodsky, Code 432   1

Director
Office of Naval Research Branch Office
536 South Clark Street
Chicago, IL. 60605
Attn: Mr. M. A. Chaszeyka   1

Commanding Officer
Naval Ship Research and Development
  Center
Bethesda, MD. 20034
Attn: W. E. Smith, Code 1576   1

Defense Documentation Center
Cameron Station
Alexandria, VA. 22134   12

The Analytic Sciences Corp.
6 Jacob Way
Reading, MA. 01867
Attn: Mr. C. Price   1

Systems Control Inc.
1801 Page Mill Road
Palo Alto, CA. 94304
Attn: Dr. E. Hall   1

Commander
Naval Sea Systems Command
Washington, DC. 20362
Attn: Mr. R. P. Dilts
         NAVSEA 0323   1

Commanding Officer
Naval Ship Engineering Center
Washington, DC. 20362
Attn: NSEC 6165   1

Prof. A. E. Bryson, Jr.
Chairman, Dept. of Aeronautics and Astronautics
Stanford University
Stanford, CA. 94305   1

Prof. J. V. Cornacchio
School of Advanced Technology
State Univ. of New York at Binghamton
Binghamton, NY. 13901   1

CDR. Bruce C. Skinner
Chief, Marine and Ocean Engineering Section
U.S. Coast Guard Academy
New London, CT. 06320   1

Dr. Rameswar Bhattacharyya
Director of the Naval Architecture Program
U.S. Naval Academy
Annapolis, MD.   1

Dr. Haruzo Eda
Davidson Laboratory
Stevens Institute of Technology
711 Hudson Street
Hoboken, NJ. 07030   1

Dr. Masataka Fujino
Department of Naval Architecture
University of Tokyo
3-1, Hongo 7-chrome
Bunkyo-ku, Tokyo, JAPAN   1

Dr. Horst Nowacki
Technishe Universität Berlin
Salzufer 17/19
1 Berlin 10,
FEDERAL GERMAN REPUBLIC   1

Dr. J. P. Hooft
Netherlands Ship Model Basin
P.O. Box 28
6700AA Wageningen, THE NETHERLANDS   1

Mathematical Hydraulics Division
Waterways Experiment Station
PO Box 631
Vicksburg, MS. 39180
Attn: Mr. Thomas D. Ankeny   1

Prof. Dr.-Ing. H. Schneekluth
Technishe Hochschule Aachen
Templergraben 55
51 Aachen, FEDERAL GERMAN REPUBLIC   1

Office of Research and Development
Maritime Administration
Department of Commerce
Washington, DC. 20230   1

Prof. Tor Vinje
Institutt for Skipshydrodynamik
N-7034-Trondheim NTH
NORWAY   1

Prof. J.R. Pauling
Dept. of Naval Architecture
University of California
Berkeley, CA. 94720   1

Dr. Charles C. Bates, G-DS/62
U.S. Coast Guard Headquarters
400 Seventh St., S.W.
Washington, DC.   1

Prof. William F. Powers
Department of Aerospace Engr.
University of Michigan
Ann Arbor, MI. 48109   1

Dr. John Ware
Operations Research, Inc.
1400 Spring Street
Silver Spring, MD.   20910   1

American Bureau of Shipping
45 Broad Street
New York, NY. 10004
Attn: Mr. Stanley Stiansen   1

Prof. M.A. Abkowitz
Dept. of Ocean Engineering
Massachusetts Institute of
 Technology
Cambridge, MA.   02139   1